Miocene climate cooling and aridification of Antarctica may have enhanced syn-extensional magmatism in the western Ross Sea

Article *in* Global and Planetary Change · August 2024

DOI: 10.1016/j.gloplacha.2024.104538

CITATIONS
0

READS
75

6 authors, including:

Marco Fioraso
Università degli Studi di Siena
2 PUBLICATIONS **0** CITATIONS
SEE PROFILE

Pietro Sternai
Università degli Studi di Milano-Bicocca
105 PUBLICATIONS **1,797** CITATIONS
SEE PROFILE

Valerio Olivetti
University of Padova
43 PUBLICATIONS **941** CITATIONS
SEE PROFILE

Massimiliano Zattin
University of Padova
198 PUBLICATIONS **4,873** CITATIONS
SEE PROFILE

Global and Planetary Change 240 (2024) 104538

Contents lists available at ScienceDirect

Global and Planetary Change

journal homepage: www.elsevier.com/locate/gloplacha

Miocene climate cooling and aridification of Antarctica may have enhanced *syn*-extensional magmatism in the western Ross Sea

Marco Fioraso [a,*], Pietro Sternai [b,c], Valerio Olivetti [d], Maria Laura Balestrieri [e], Massimiliano Zattin [d], Gianluca Cornamusini [a]

[a] Department of Physical Sciences, Earth and Environment, University of Siena, Siena, Italy
[b] Department of Earth and Environmental Sciences, University of Milano-Bicocca, Milano, Italy
[c] GFZ German Research Centre for Geosciences, Potsdam, Germany
[d] Department of Geosciences, University of Padova, Padova, Italy
[e] Institute of Geosciences and Earth Resources, Italian National Research Council, Firenze, Italy

ARTICLE INFO

Editor Name: Prof. Liviu Matenco

Keywords:
Surface–deep Earth interactions
Ultra-slow rifting
Miocene climate
Syn-rift magmatism
Antarctica

ABSTRACT

Continental rift systems are commonly characterized by volcanism with parental basaltic magmas sourced from the mantle. Erosion of the rift shoulders and sedimentation in the adjacent basins can affect the stress and thermal fields at depth, thereby affecting partial mantle melting. However, the sensitivity of magmatic activity to such surface forcing is elusive. Geological observations from the western Ross Sea, Antarctica, suggest rift onset in the Cretaceous with a transition from wide-rifting to narrow-rifting at the boundary between the Antarctic craton and the Transantarctic Mountains. Miocene climate cooling during rifting in the western Ross Sea, in addition, leads to an abrupt decrease in sedimentation rate, synchronous to the emplacement of the McMurdo Volcanic Group. This represents the largest alkali province worldwide, extending both inland and offshore of Transantarctic Mountains and western Ross Sea, respectively. Here, we use coupled thermo-mechanical and landscape evolution numerical modeling to quantify melt production in slowly stretching rift basins due to changes in erosion/deposition rates. The model combines visco-elasto-plastic deformation of the lithosphere and underlying mantle during extension, partial rock melting, and linear hillslope diffusion of the surface topography. The parametric study covers a range of slow extension rates, crustal thicknesses, mantle potential temperatures and diffusion coefficients. Numerical simulations successfully reproduce the ~150–200-km-wide extension of western Ross Sea and Miocene-to-present asthenospheric melt production (McMurdo Volcanic Group). Results further show that slow rifts magmatism is highly sensitive to sediment deposition within the basin, which inhibits mantle decompression melting and delays the crustal breakup. Regional climate-driven sedimentation rate changes are thus likely to have affected the *syn*-rift magmatic history of the western Ross Sea, Antarctica, supporting the relevance of interactions between surface and deep-seated processes across extensional settings.

1. Introduction

Continental rifting and associated extensional sedimentary basins testify significant interactions between lithospheric strain, magmatism and surface processes (White and McKenzie, 1989; Buck, 1991; Brun et al., 1999; van Wijk et al., 2001; Ziegler and Cloetingh, 2004). For instance, continental rifting generates prominent topography and the flux of eroded material from rift flanks to the extensional rift basin, i.e., surface processes, affects the flow of the viscous lower crust (Burov and Cloetingh, 1997; Burov and Poliakov, 2001), lithospheric flexure (e.g., Watts, 2001), the thermal structure at depth via surface blanketing (Bialas and Buck, 2009), and the overall tectonic strain (e.g., van der Beek et al., 1995; Burov and Cloetingh, 1997; Burov and Poliakov, 2001; Bialas and Buck, 2009; Sternai et al., 2021). Since the production and transfer of magma across extensional settings depends on the stress and thermal fields at depth (McKenzie and Bickle, 1988; White and McKenzie, 1989), the link between magmatism and climate-driven surface processes is attracting increasing attention and involves

* Corresponding author.
E-mail address: m.fioraso@student.unisi.it (M. Fioraso).

https://doi.org/10.1016/j.gloplacha.2024.104538
Received 13 April 2024; Received in revised form 2 August 2024; Accepted 5 August 2024
Available online 12 August 2024

multiple tectonic settings (e.g., Cloetingh et al., 2023; Sternai, 2023). Unloading caused by deglaciation can affect the rate of partial decompression mantle melting (Jull and McKenzie, 1996), an effect that may even be relevant on a global scale and regardless of the tectonic regime (Huybers and Langmuir, 2009). Erosion and sea level changes also exerts a control on surface loading and unloading during glacial-interglacial cycles, thereby affecting rock melting and degassing from the solid Earth (e.g., Huybers and Langmuir, 2009; Sternai et al., 2016; Sternai, 2020; Stüwe et al., 2022).

Because feedbacks between surface, lithosphere and asthenosphere dynamics also involve climate and the long-term carbon cycling via magmatic emissions of CO_2 and other greenhouse gases (e.g., Brune et al., 2017; Sternai et al., 2020; Sternai, 2023; Cloetingh et al., 2023), assessing the influence of surface processes on *syn*-rift magmatism is timely and important. Extensional geodynamics and their relationships with surface processes are commonly investigated across medium to fast Atlantic-type margins or narrow regions of oceanic crust exposed at the sea floor (e.g., the Red Sea) (e.g., Ziegler and Cloetingh, 2004; Stüwe et al., 2022; and references therein), whereas slow, widespread, and long-lasting rift systems have been less explored (e.g., van Wijk and Cloetingh, 2002). The West Antarctic Rift System region in Antarctica is a large, slow and long-lasting continental rift system (Siddoway, 2008; Davey et al., 2016; Jordan et al., 2020) compared to other extensional systems worldwide (e.g., Bowling and Harry, 2001, and references therein). The Ross Sea and its western rift flank, the Transantarctic Mountains, are subject to climate variations throughout the Cenozoic, involving in particular a major shift from relatively warm and wet to extremely arid and cold conditions (Lewis et al., 2008; Levy et al., 2019), which set the pace of Transantarctic Mountains erosion and sediment discharge to extensional basins.

Extensional settings are typically studied as a function of extension rate (e.g., Bowling and Harry, 2001; van Wijk and Cloetingh, 2002; Dick et al., 2003; Schmeling, 2010; Koptev et al., 2018). Here, we use numerical thermo-mechanical geodynamic modeling and the Ross Sea as a natural case study to assess the sensitivity of extensional magmatism to surface processes in ultra-slow rift systems. Spreading velocities lower

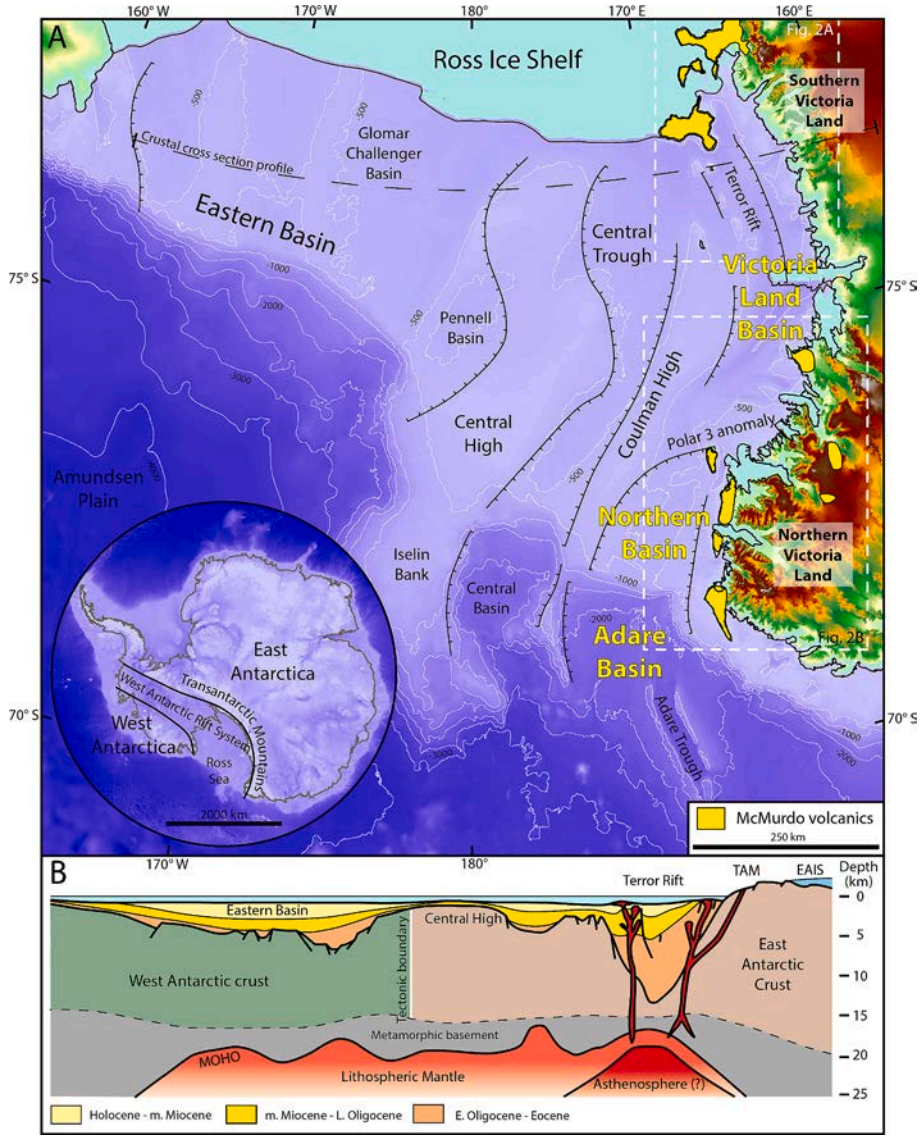

Fig. 1. Map of Antarctica and the Ross Sea. (A) Map of the Ross Sea showing structural lows and highs between West Antarctica and the Transantarctic Mountains front. Topography and bathymetry from BedMachine DEM (Morlighem et al., 2020). The bathymetric lines are spaced at intervals of 500 m. (B) Crustal-scale cross-section modified from Busetti et al. (1999) and Huerta and Harry (2007) showing the general structure of the boundary between West Antarctic Rift System and East Antarctic craton. The tectonic boundary between West Antarctic and East Antarctic crust is taken from Tinto et al. (2019), the Moho is from Busetti et al. (1999). Sedimentary units are bounded by RSU4 (middle Miocene) and RSU6 (Early Oligocene) unconformities (Levy et al., 2019; McKay et al., 2022).

than 12 mm/yr in ocean ridges are classified as "ultra-slow" (Dick et al., 2003), and in this work we encompass a range of extension velocities (2.5 to 5.5 mm/yr) below the proposed threshold. A ~ 150–200 km-wide ultra-slow extension reproduced in numerical simulations describes the Cenozoic narrow rifting occurring on the western portion of the West Antarctic Rift System and its associated *syn*-rift magmatism.

2. Geological background

The western Ross Sea (WRS) represents the westernmost portion of the continental shelf between East and West Antarctica bounded by a high-elevation rift flank, the Transantarctic Mountains (TAM) (Fig. 1). The WRS can be divided into two sectors, the Adare Basin and Northern Basin in the north, and the Victoria Land Basin in the south (Fig. 1). The geology and physiography of the Ross Sea continental shelf depends on the juxtaposition of the West Antarctica lithosphere, and the East Antarctica cratonic lithosphere (Tinto et al., 2019) (Fig. 1B). The region was subject to crustal stretching since the initial breakup of Gondwana in the Early-Middle Jurassic (Fitzgerald and Baldwin, 1997; Fitzgerald, 2002; Davey et al., 2016), forming the West Antarctic rift system, a ~600 km wide thinned continental crust dominated by a low-lying morphology (Jordan et al., 2020).

Extension in the West Antarctic Rift System can be divided into two tectonic phases (Siddoway, 2008). The first phase (wide rifting) is a prolonged period of broadly distributed extensional strain since the Early Cretaceous. The second phase (narrow rifting) involves localized extensional strain at the boundary between the East Antarctic craton and the thin and hot West Antarctic lithosphere since the Paleogene (Huerta and Harry, 2007; Harry et al., 2018; Jordan et al., 2020). The progressive westward migration and localization of the deformation toward the WRS during the Neogene is likely related to the thermal evolution of the West Antarctic Rift System (Huerta and Harry, 2007).

The TAM represent the remnants of crust thickened during Paleozoic convergent tectonics (Bialas et al., 2007) (Fig. 1). After the onset of wide rifting, the TAM acted as a high-elevation rift flank and a topographic divide between the Ross Sea and the East Antarctic craton. Major crustal anisotropies, due to the presence of inherited structures developed within the Ross Orogeny, contributed to set the overall structural architecture of the TAM (Fitzgerald, 2002; Goodge, 2020) and influenced the rifting evolution (Brune et al., 2023). Weakened Paleozoic shear zones arranged the general physiography of the high-elevation margin in structural domains that were reactivated by Cenozoic transtensive tectonics (Salvini et al., 1997). Thermochronological data suggests multiple phases of exhumation in the TAM starting from the early Cretaceous (Fitzgerald and Goodge, 2022). Nevertheless, only the last Cenozoic exhumation phase is well described in the sedimentary record of the Ross Sea (Olivetti et al., 2013).

2.1. Continental rifting

The main rifting phase occurred in the Cretaceous between approximately 105 and 71 Ma (Siddoway et al., 2004). Successively, an ultra-slow seafloor spreading phase, constrained by magnetic anomalies, occurred between 61 and 53 Ma in the Central Basin (Davey et al., 2022) and between 43 and 26 Ma in the Adare Trough (Granot and Dyment, 2018). In addition to E-W extension along the TAM front, transtensive

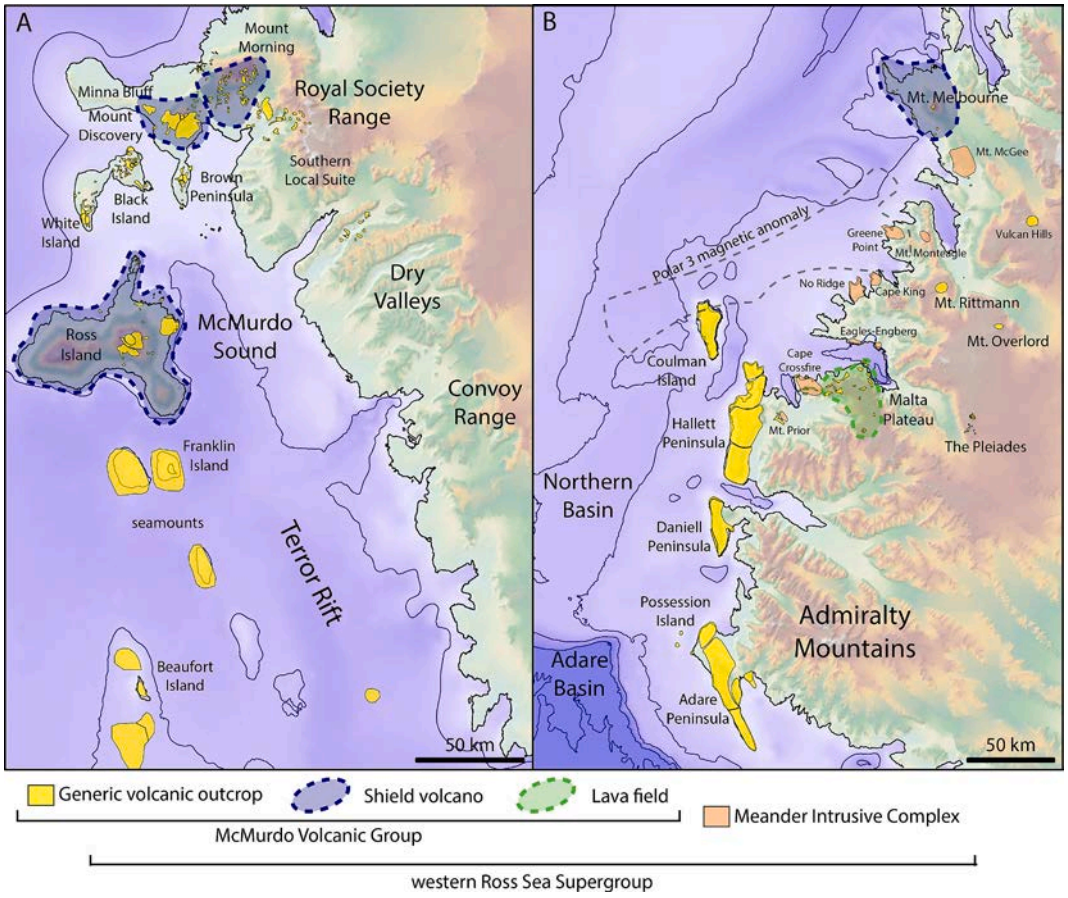

Fig. 2. Maps showing the spatial distribution of McMurdo volcanics and Meander Intrusive Complex. (A) Volcanic outcrops in Victoria Land Basin region; (B) volcanic-subvolcanic outcrops in northern Victoria Land, on the western side of Northern Basin and Adare Basin. Polygons are redrawn from Rilling et al. (2009), Martin et al. (2021), Rocchi and Smellie (2021), Smellie and Martin (2021), Smellie and Rocchi (2021). Shield volcanoes and the Malta Plateau lava field belong to McMurdo Volcanic Group. The Polar 3 magnetic anomaly (Ferraccioli et al., 2008) is shown by the dashed grey line.

reactivation took place acting as intraplate termination of transform shear and propagating into inherited Paleozoic shear zones. The propagation of strike-slip faults into the WRS resulted in oblique rifting, which has been proposed to be active at least since the Eocene (Rossetti et al., 2006). A dextral transtension is reported in the Terror Rift sector at ~26 Ma (Sauli et al., 2021) (Figs. 1, 2).

The Adare Basin shows a comprehensive total extension of ~170 km (Wilson and Luyendyk, 2009), with an extension rate of ~10–12 mm/yr (Cande et al., 2000; Davey et al., 2016) constrained between 43 and 26 Ma by seafloor magnetic anomalies. Previous modeling of the Victoria Land Basin sector proposed ~95 km of stretching since ~34 Ma (Davey and De Santis, 2006), corresponding to an average extension velocity of ~2.7 mm/yr. Alternatively, Wilson and Luyendyk (2009) suggest ~170 km of stretching since 38 Ma at ~4.5 mm/yr. In general, a southward decreasing trend of extension rate from the Adare Basin to the Victoria Land Basin is observed (Davey et al., 2016). The beginning of extension in the Victoria Land Basin is assumed to be synchronous to that in the Northern Basin, although the tectonic activity continues until recent times in the Terror Rift (see Fig. 1) (Sauli et al., 2021). The Adare Basin-Northern Basin represent a wide zone of continent-ocean transition

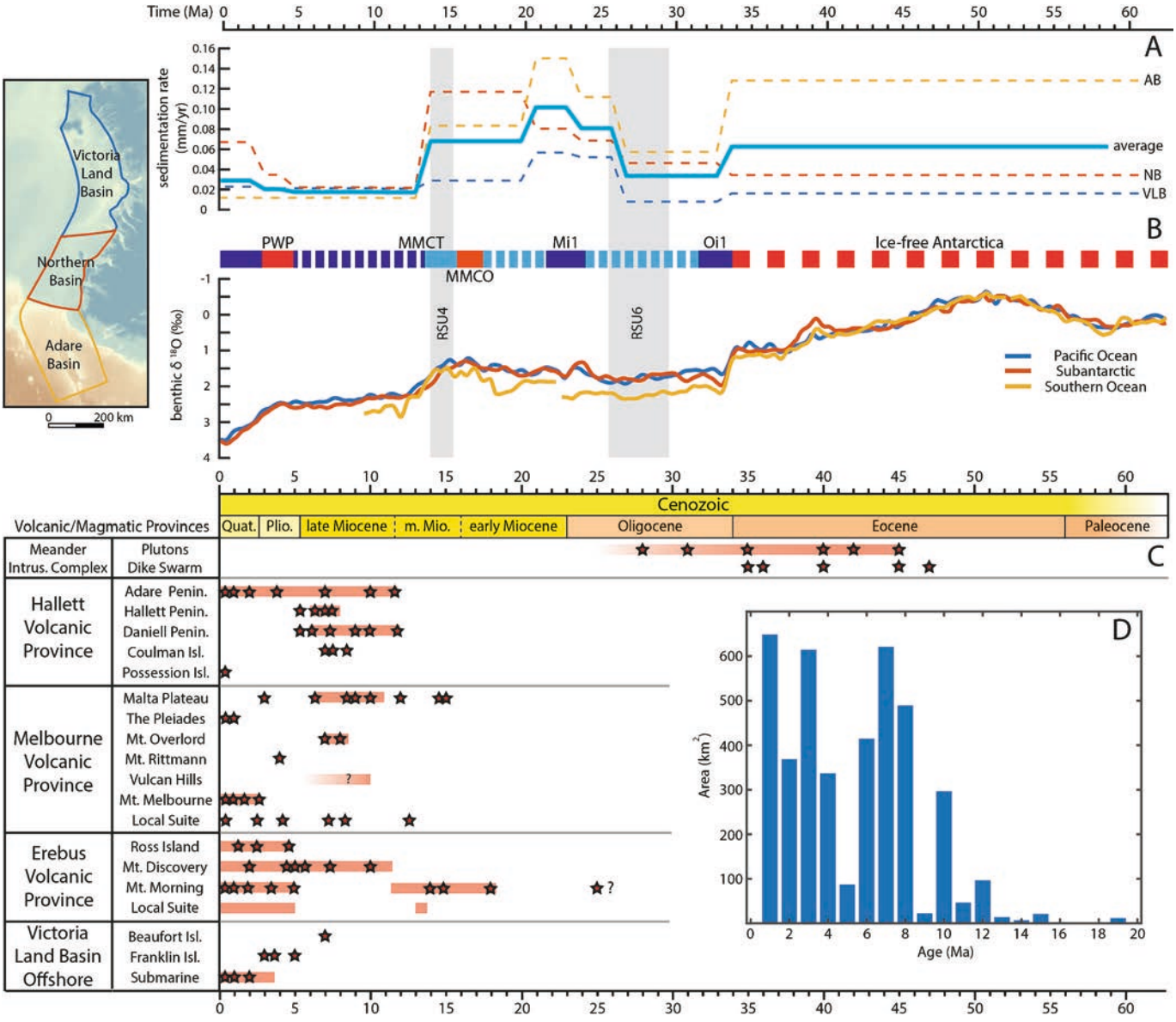

Fig. 3. Chronological summary correlating climate, ice-sheet evolution, sedimentation and volcanic/magmatic events. (A) Sedimentation rates for Victoria Land Basin (VLB), Northern Basin (NB), Adare Basin (AB). Grey-shaded field indicates time intervals corresponding to Ross Sea Unconformities 4 and 6 (Levy et al., 2019; McKay et al., 2022). (B) Ice sheet evolution (McKay et al., 2022) and far-field benthic oxygen isotopes ratio (Cramer et al., 2009). Colored bar on the ice-sheet evolution scheme: red indicates relatively warm climate (terrestrial warm-based glaciers), light blue indicates cool climate (variable terrestrial and marine ice sheets), blue indicates cold to very cold climate (glacial maxima). (C) Volcanic/magmatic events recorded in the western Ross Sea Supergroup outcrops (Martin et al., 2021; Rocchi and Smellie, 2021; Smellie and Martin, 2021; Smellie and Rocchi, 2021) and dredges (Rilling et al., 2009). Orange stripes in magmatism chronological chart indicate periods of inferred continued activity. (D) Surface distribution of outcropping volcanic rocks since Early Miocene (Fig. 2A-B) of McMurdo Volcanic Group taken from published maps and age determinations (Smellie and Martin, 2021; Smellie and Rocchi, 2021). The map in the rectangle shows modern-day perimeter of the basins considered by this study; the topography-bathymetry is taken from BedMachine (Morlighem et al., 2020). In panel (D) surfaces are underestimated due to ice-covered outcrops not entirely considered in this work. Abbreviations: Oi1, Eocene-Oligocene glaciation; Mi1, Oligocene-Miocene Glaciation; MMCO, Middle Miocene Climate Optimum; MMCT, Middle Miocene Climate Transition, PWP, Pliocene Warm Period. (For interpretation of the references to colour in this figure legend, the reader is referred to the web version of this article.)

characterized to abundant intrusions and crustal growth (as for the Central Basin oceanic crust modeling, Davey et al., 2022). Aeromagnetic anomalies are uniform through the continental edge linking the Northern and Adare basins genetically (Davey et al., 2016). The ENE-trending boundary between the Northern Basin and Victoria Land Basin is inferred to represent a transfer zone accommodating different motion between the two basins. Along this boundary a broad magmatic anomaly, the Polar 3 anomaly (Fig. 2B), suggests the presence of magmatic intrusions (Rocchi et al., 2002) or even the possible formation of oceanic crust (Davey et al., 2016).

During the early rifting phase in the Ross Sea, north-striking grabens were formed and filled with sediments since at least the Cretaceous-Paleogene (Cooper et al., 1991). The RSU6 unconformity (McKay et al., 2022) represents the boundary between the sediment infill during the wide extensional tectonic phase (Cretaceous-Paleogene) and the overlaying sediments, undeformed in Eastern Basin and Central Trough (Fig. 1). Seismic data display the presence of km-thick sequences laying between the acoustic basement and the RSU6 (see Fig. 1B) (McKay et al., 2022). The RSU4 unconformity, 14.1–15.8 Ma (Levy et al., 2019), marks the most recent tectonic activity in the Terror Rift (in the western sector of the Ross Sea). This last phase is ultimately associated with the presence of magmatic submarine intrusions and onshore/offshore volcanism promoted by rift-bounding faults crosscutting the entire *syn*-rift sequence.

2.2. Regional magmatism

In the WRS and TAM, rift-related magmatic products occurred for the first time around ~48 Ma in Northern Victoria Land between Mt. Melbourne and the Hallett Peninsula (Rocchi et al., 2002), forming the Meander Intrusive Group (Fig. 2B), a series of Eocene to early Miocene plutonic and subvolcanic rocks (Fig. 3). After ~14 Ma (Fig. 3) the majority of magmatism was widely distributed in the region (Panter and Martin, 2021) forming the McMurdo Volcanic Group (Kyle, 1990a) (Fig. 2A, B). It can be divided in three main provinces: (1) the Hallett Volcanic Province (McIntosh and Kyle, 1990) and (2) the Melbourne Volcanic Province (Kyle, 1990b) in Northern Victoria Land (Fig. 2B), and (3) the Erebus Volcanic Province in the McMurdo Sound area of the southwest Ross Sea (Fig. 2A). Considering all the Cenozoic magmatic and volcanic products in the WRS, the western Ross Supergroup (Rocchi et al., 2002; Rocchi and Smellie, 2021) represents one of the most extensive alkali provinces in the world, with volcanic centers and plutons spreading for >1000 km across the Ross Sea and TAM. Alkaline magmatism is characterized by its development along a complete transect of continent-ocean transition from the Adare Basin seamounts to the volcanic edifices exposed onshore along the TAM margin (Durkin et al., 2023).

Plutons of the Meander Intrusive Group generally have a syenitic compositions, while dykes cutting both plutons and Paleozoic basement show a greater compositional variability from alkali basalts to trachyte-rhyolite (Rocchi and Smellie, 2021). McMurdo volcanics show three main morphologies on the TAM coast (Kyle, 1990a): basaltic shield volcanoes, trachytic-phonolitic stratovolcanoes and basaltic scoria cones or lava flow fields. The geochemical signature, common to all the western Ross Supergroup magmatic/volcanic products, indicates an ocean island basalt-like composition, with high μ-like isotopic ratios (Panter et al., 2018; Durkin et al., 2023). The origin of West Antarctic Rift System magmas, including the possibility of mantle plumes involvement, is debated (e.g., Storey et al., 1999; Rocchi et al., 2002). Recent interpretations, however, suggest that decompression melting of carbonate-rich subduction-related material (Panter et al., 2018) generated in convergence settings since Neoproterozoic (Goodge, 2020) plays a role. Due to ultra-slow rifting evolution, metasomatic enrichment of lithospheric mantle during the wide rifting phase affects decompression melting that occurred later, between the Eocene and Neogene (Panter et al., 2018).

2.3. Climatic evolution and sedimentation rates

Since Cretaceous to Eocene, Antarctic climate was warm and humid with mean annual temperature between ~10–15 °C (McKay et al., 2022). Glaciers are expected in high elevation terranes of East Antarctica, e.g., around peaks of the TAM (Paxman et al., 2019; Barr et al., 2022) where high-altitude cirques formed in the Mesozoic were detected. Pre-glacial erosion was mostly affected by coeval uplift of the TAM and Paleogene paleotopography (Lindeque et al., 2016; Paxman et al., 2019). Sedimentation in WRS basins occurred at variable rates, 0.01–0.13 mm/yr (Fig. 3A). A strong decrease in temperature occurred between middle to late Eocene (~ 37 Ma) (Fig. 3B), when the majority of TAM cirques could possibly be occupied by ice (Barr et al., 2022).

The first continental-scale ice sheets developed at the Eocene-Oligocene boundary due to a combination of optimal orbital configuration, decreasing atmospheric CO_2 and tectonic opening of the Southern Ocean gateways (McKay et al., 2022). Cooling and aridification in terrestrial areas occur in the early Oligocene (McKay et al., 2022). Coeval to glacial expansion, a decrease in sedimentation rates occurred due cooler climate conditions (Fig. 3A). Successively, a shift to warmer climate led to the Miocene Climate optimum (Levy et al., 2019). The presence of wet-based glaciers is suggested by plant and animal fossils, confirming positive mean annual temperatures in the TAM (Lewis et al., 2008). A rapid acceleration in sedimentation rate is recorded all along WRS basins, up to 0.15 mm/yr in Adare Basin from early Miocene to middle Miocene, reflecting the response of fluvio-glacial sedimentary systems to a warmer climate and a high variability in ice-sheet dynamics (Levy et al., 2019) (Fig. 3A).

Rapid isotopic excursion in the middle Miocene marks the transition to hyper-arid polar climate conditions (Sugden and Denton, 2004; Lewis et al., 2008). In the stratigraphic record of the Ross Sea, a well-constrained glacial unconformity, the RSU4 (14.1–15.8 Ma, after Levy et al., 2019), corresponds to marine-based advance of the East Antarctic Ice Sheet, consistent with the Middle Miocene Climate Transition (Levy et al., 2016) (Fig. 3). The establishment of a permanent East Antarctic Ice Sheet and stable arid conditions in terrestrial environments after the middle Miocene is debated (Verret et al., 2023). Nevertheless, the regional stratigraphy suggests a two-fold (Victoria Land Basin) up to ten-fold or stronger (Northern Basin) decrease in sediment discharge efficiency since the middle Miocene (Lindeque et al., 2016; Hochmuth et al., 2020), reaching sedimentation rate close to 0.01 mm/yr (Fig. 3A). Along the TAM, a stable permafrost and extremely low erosion rates are suggested by the landscape, which is a relic of Miocene times (Sugden and Denton, 2004). A general northward increase in sedimentation rates variability through the Cenozoic is observed, reflecting differences in landscape evolution as suggested by contrasting TAM topography along strike (Olivetti et al., 2018; Balestrieri et al., 2020).

3. Methods

Numerical models are used to assess the impact of surface processes on the magmatic activity of slow rift settings. We report here the main equations in our numerical models, but the reader can also refer to Gerya (2019) or Sternai (2020) and references therein for additional detail. We opted for a bidimensional model to address the coupling between rifting tectonics, surface processes, and rock melting with reduced computational costs, as often done by previous studies (e.g., Bowling and Harry, 2001; van Wijk et al., 2001; Bialas and Buck, 2009; Schmeling, 2010). The code is based on a version of the bi-dimensional visco-elasto-plastic thermo-mechanical ELVIS code family (Gerya and Yuen, 2007), implemented to account for surface processes based on a simple linear downslope diffusion law applied to the evolving topography (Sternai, 2020) such that,

$$\partial z/\partial t = k\nabla^2 z \quad (1)$$

where $\partial z/\partial t$ is the variation of the surface elevation due to erosion or sediment deposition in time, $\nabla^2 z$, is the topographic curvature, and the diffusivity, k, is used to scale the imposed erosion/deposition rates. The diffusion law in Eq. (1) is simplistic but enables us to swiftly account for erosion of rift flanks and sedimentation in basins. Eq. (1) is solved numerically by integration on the discrete surface topography (Gerya and Yuen, 2003), which is updated at each timestep to allow the calculation of surface load changes.

The extensional strain of the lithosphere is based on a rheological model that accounts for visco-elasto-plastic deformation conserving the mass, momentum and energy within the model, such that,

$$\begin{cases} \partial\rho_{eff}/\partial t + div(\rho_{eff} v) = 0 \\ div(\sigma') - \nabla P + \rho_{eff} g = 0 \\ \rho_{eff} C_p \dfrac{DT}{Dt} - div(c\nabla T) = H_r + H_s + H_a + H_l \end{cases} \quad (2)$$

where ρ_{eff} is the effective density of rocks (see Eq. (4)), v, is the velocity vector, σ', is the deviatoric stress tensor, g, is the gravity acceleration, C_p, is the specific heat capacity, T, is temperature, c, is the thermal conductivity, H_r, H_s, H_a, H_l are respectively the radiogenic, shear, adiabatic, latent heat production. The elastic behavior is given by linearly related stress and strain, the plastic behavior depends on the relation between brittle rock strength and pressure, the viscous behavior is thermally activated and depends on the relation between stress and strain rate regulated by viscosity (the resistance of material to shear deformation), as described in Gerya (2019).

Partial rock melting and crystallization of magmas occur between the wet solidus and dry liquidus curves of lithospheric and asthenospheric rocks (Table 1). The melting fraction, ξ, increases linearly with temperature at constant pressure:

$$\begin{cases} \xi = 0 \; at \; T \le T_s \\ \xi = \dfrac{T - T_s}{T_l - T_s} \; at \; T_s < T < T_l \\ \xi = 1 \; at \; T \ge T_l \end{cases} \quad (3)$$

where T_s is the solidus temperature, and T_l is the liquidus temperature. The effective density of partially molten material, ρ_{eff}, is calculated as:

$$\rho_{eff} = \rho_s\left(1 - \xi + \xi\left(\rho_s^0/\rho_l^0\right)\right) \quad (4)$$

where ρ_s^0 and ρ_l^0 are the standard densities of solid and molten rocks and ρ_s is the density of solid rocks at given pressure/temperature conditions. The effective viscosity, η, of partially molten rocks whose melting fraction is larger than 0.1 is set equal to 10^{16} *Pa s*, which allows accounting for relatively large viscosity jumps between materials avoiding numerical issues. The viscosity range is set between 10^{16} *Pa s* and 10^{25} *Pa s*. All the material properties used in the numerical model are listed in Table 1.

Eqs. (1–4) are coupled via stress, temperature and velocity continuity conditions, adopting the finite-differences approximation scheme and a fully staggered bi-dimensional grid (Gerya and Yuen, 2007; Gerya, 2019). The initial domain (Fig. 4) measures 400 × 300 km in the x and y dimensions, resolved by 161 × 61 grid points respectively, distributed on an irregular Eulerian grid. 400 × 300 Lagrangian markers are randomly distributed in the x and y dimensions and used for advecting the material properties, which are interpolated onto the Eulerian grid via a 4th-order Runge-Kutta interpolation scheme. The velocity boundary conditions are free slip at all boundaries (x = 0 and x = 400 km; y = 0 and y = 300 km). The left and right boundaries (x = 0 and x = 400 km) also account for equally distributed x-parallel velocities, defining the extension rate within the model. The lower boundary (y = 300 km) also accounts for y-parallel velocity to compensate for horizontal extension and ensure global mass conservation. The top surface of the lithosphere is calculated dynamically as an internal free surface through a 10 km thick layer of "sticky air". The initial temperature gradient in the asthenospheric mantle is 0.4 °C/km (adiabatic). The thermal boundary conditions are 0 °C for the upper boundary and between 1367 and 1477 °C on the lower model boundary. A seed of thermally weak material with 2 km radius is imposed on the Moho in the center of the model domain to initiate the lithospheric rupture. At each time step, which is limited by the Courant criteria (Courant, 1928), the topography and topographic load changes due to erosion and/or sediment deposition are computed.

The parametric study focuses on a set of values for extensional velocity, mantle potential temperature, T_p, (sensu McKenzie and Bickle, 1988), and crust thickness, which primarily control the lithospheric stretching and the magmatic evolution in a continental rift (White and McKenzie, 1989). For each set of parameters, we perform simulations using high/low diffusivity values to explore the effects of different surface processes efficiency, scaling the erosion/deposition rates consistently with the WRS sedimentary record. In particular, we use sediment thickness estimates by Hochmuth et al. (2020) to derive sedimentation rates every 1 Myr dividing the sediment volumes by the basin surface area. We consider the Mesozoic-Cenozoic boundary as the inception of sedimentation in the WRS to calculate a sedimentation rate estimate for pre-Eocene-Oligocene sediments. We explore a range of surface processes efficiencies that encompasses the rate of landscape denudation in northern-southerns Victoria Lands, in agreement with sedimentation rates within the WRS since at least the Oligocene (Paxman et al., 2019). Erosion/sedimentation rates are set as constant (time-independent) for each simulation. Imposing $k = 1$ m^2/s, erosion/deposition rates result higher than values suggested by the geological record, but useful to set a high-end reference simulation. The simulations address the extension of a thin lithosphere for ~60 Myr, a time interval similar to the duration of narrow lithospheric stretching in the WRS (Wilson and Luyendyk, 2009; McKay et al., 2022). We performed 43 runs (Table 2), changing: (1) the extension velocity, from 2.5 to 5.5 mm/yr, to obtain at least ~150–200 km of extension; (2) the thickness of the crust, from 25 to 30 km; (3) the potential mantle temperature from 1250 to 1360 °C; (4) the efficiency of surface processes from 1 to 0.01 mm/yr. The melt volume data extracted by numerical simulations are displayed in m^2, considering the bi-dimensional nature of our numerical experiments.

4. Results

4.1. Model results

The reference model (Fig. 5) for an ultra-slow rift with efficient surface processes and a 25 km thick crust evolves in two phases. In the first phase, the extensional strain is broadly distributed across the upper crust, whereas necking occurs in the lithospheric mantle until its complete rupture (Fig. 5B). In the second phase, the stretching is progressively localized in the crust leading to lithospheric breakup (Fig. 5C), defined as the first contact between the asthenosphere and sediments through rupturing of the crust (shown by the vertical dotted line in Fig. 5). During the rift evolution, early partial melting of the lowermost crust (Fig. 5B) at direct contact with the upwelling asthenosphere is followed by decompression partial melting of the asthenosphere due to adiabatic upwelling (Fig. 5C).

The extension velocity exerts a primary control on (1) rifting duration, (2) the onset of magmatism, and (3) the *syn*-rift melts volume. For the reference lithospheric structure (Figs. 4, 5), slower stretching by 40% (from 3.5 to 2.5 mm/yr) increases the time to the breakup by about 20 Myr (Fig. 6). Slower extension caused a decrease in the rates of lithospheric necking, asthenospheric upwelling and partial decompression melting (see the difference in melt volumes in Fig. 6). In models stretching at 2.5 mm/yr, asthenospheric melting commonly begins around or after the breakup event (Fig. 6), whereas simulations extending at 3.5 mm/yr lead to about two orders of magnitude more

Table 1
Material properties used in numerical simulations. ρ_0 (of solid and molten material) is the density, E_a is the activation energy, V_a is the activation volume, n is the stress exponent, C is the cohesion, Qz. and Ol. correspond to the abbreviations of Quartzite and Olivine, ϕ_{eff} is the effective internal friction angle, c is the thermal conductivity, μ is the Young's modulus, ν is the Poisson's ratio, C_p is the specific heat capacity, H_r is the radiogenic heat production, α and β are the thermal expansion and compressibility, respectively, Q_l is the lithology-related latent heating, and T_s and T_l are the solidus and liquidus temperature, respectively. Values are taken from Turcotte and Schubert (2016), Gerya (2019), Sternai (2020) and references therein.

	ρ_s^0 ρ_l^0 (kg/m^3)	Ea (kJ/mol)	Va (m^3/mol)	n	C (MPa)	Viscous flow law	sin (Φ_{eff})	C (W/m/K)	μ (GPa)	v	C_p (J/kg/K)	H_r (μW/m^3)	α (1/K)	β (1/Pa)	Q_l (kJ/kg)	$T_{solidus}$ (K)	$T_{liquidus}$(K)
Sediments	2600 (solid), 2400 (molten)	154	0	2.3	10	Wet Qz.	0.1	0.64	10	0.2	1000	2	$3 * 10^{-5}$	$1 * 10^{-11}$	300	889 + 17,900 / (P + 54) + 20,200 / (P + 54)^2 at P < 1200 MPa 831 + 0.06 * P at P > 1200 MPa	1262 + 0.09 * P
Crust	2750 (solid), 2400 (molten)	154	0	2.3	10	Wet Qz.	0.2	0.64	10	0.2	1000	1	$3 * 10^{-5}$	$1 * 10^{-11}$	300	889 + 17,900 / (P + 54) + 20,200 / (P + 54)^2 at P < 1200 MPa 831 + 0.06 * P at P > 1200 MPa	1262 + 0.09 * P
Lithospheric mantle	3300 (solid), 2700 (molten)	532	10	3.5	10	Dry Ol.	0.6	0.73	67	0.2	1000	0.022	$3 * 10^{-5}$	$1 * 10^{-11}$	400	1394 + 0.132899 * P – 0.000005104 * P^2 at P < 10,000 MPa 2212 + 0.030819 * (P – 10000) at P > 10,000 MPa	2073 + 0.114 * P
Asthenospheric mantle	3250 (solid), 2700 (molten)	532	10	3.5	10	Dry Ol.	0.6	0.73	67	0.2	1000	0.022	$3 * 10^{-5}$	$1 * 10^{-11}$	400	1394 + 0.132899 * P – 0.000005104 * P^2 at P < 10,000 MPa 2212 + 0.030819 * (P – 10000) at P > 10,000 MPa	2073 + 0.114 * P

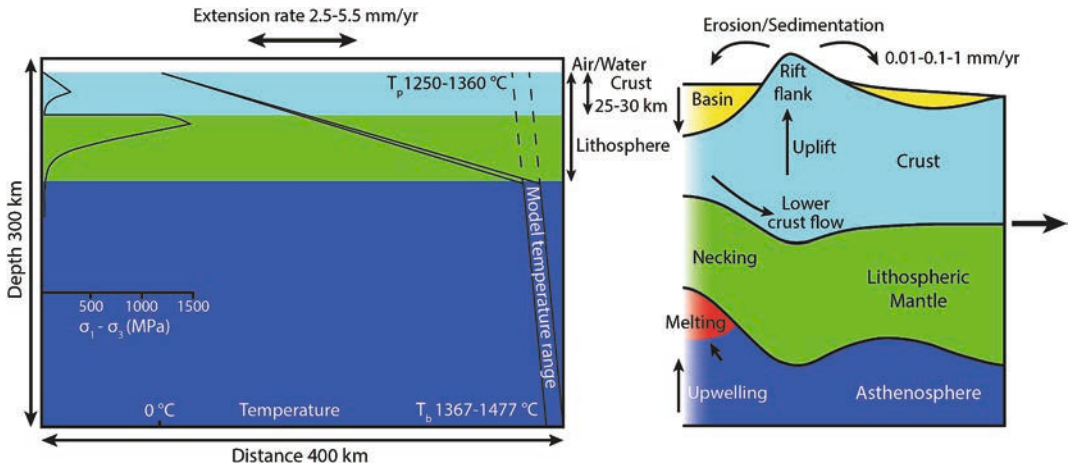

Fig. 4. On the left panel the model setup showing the initial domain, the thermal state and the yield strength profile. The strength envelope is calculated at the timestep #2 of the reference model with a strain rate of $1*10^{-15}s^{-1}$. The values indicated are used in the parametric study. Colors refer to different rock types. T_b is the temperature at the bottom of the model, T_p is the mantle potential temperature. On the right panel the graphical representation of the theoretical problem referring to feedbacks between surface processes and deep-seated processes (Cloetingh et al., 2023). Sediments from rift flank load the extensional rift basin promoting flexure and weakening of the lithosphere. A lower-crust flow from the center of the rift moves outward facilitating uplift. Extension and necking of the lithosphere promote asthenospheric upwelling causing decompression rock melting. It is noted that basin load generates an overpressure opposed to adiabatic upwelling of the mantle material.

Table 2
Summary of the parametric study conducted on a total of 43 numerical experiments analyzing multiple set of initial values for crust thickness (H_{crust}), mantle potential temperature (T_p), extensional velocities (v_e), effective diffusivity (k).

	H_{crust} (km)	T_p (°C)	v_e (mm/yr)	k (mm/yr)
RUNS 1–10	25	1310–1360	2.5	0.01–1
RUNS 11–24	25	1300–1340	3.5	0.01–1
RUNS 25–28	25	1270–1290	4.5	0.01
RUNS 29–31	25	1250–1270	5.5	0.01
RUNS 32–43	30	1300–1340	3.5	0.01–1

partial decompression mantle melting before breakup.

The mantle temperature controls the generation of asthenospheric melts. Progressive 10 °C increase in mantle potential temperature leads to a large increase in the amount of generated melts, with hotter simulations anticipating the beginning of melting (Fig. 7). Crustal melting is mostly controlled by the crust thickness and the Moho temperature before complete lithospheric mantle rupturing (Fig. 5B). In comparison with the 25 km thick reference crust, simulations with a 30 km thick crust involves a tenfold increase in crustal melting at its peak and delayed continental breakup by ~8 Ma due to higher Moho temperatures, which promote distributed lower crustal ductile deformation (Fig. 7). The amount and timing of decompression mantle melting is largely independent of the initial crustal thickness and remain directly related to the mantle potential temperature.

In ultra-slow rift systems, surface process efficiency, that is the ability to deliver sediments from uplifted rift flanks to the basin, affects both the magmatic evolution and timing of breakup. In set-ups with a 25 km-thick crust, an increase in surface erosion/deposition rates from 0.01 to 1 mm/yr leads to twice as much crustal partial melting (Fig. 8A). In set-ups with a 30 km-thick crust (Fig. 8B), however, the effect of surface processes on crustal melting is negligible. In hot (T_p = 1340 °C) simulations shown in Fig. 8A and B, higher sedimentation rates inhibit asthenospheric melting during later rifting and shortly before the breakup. During the early stages of melting, the effect of surface processes is difficult to assess (Fig. 8A, B). In slightly cooler simulations (T_p = 1310 °C) and a 25-km-thick crust, asthenospheric decompression melting is inhibited by efficient surface processes (Fig. 8C). A nearly ~25% difference in cumulative melt volume is observed between a high sedimentation rate model (1 mm/yr, blue column Fig. 8C) and a low sedimentation rate model (0.01 mm/yr, orange column Fig. 8C). Whereas in models with a 30 km thick crust (see Fig. 8D), the reduction of asthenospheric decompression melting due to efficient surface processes is prominent even before the breakup.

Fig. 9 provides a visual representation of the role of surface processes in affecting decompression mantle melting. Lowering the mantle potential temperature below 1340 °C and 1300 °C prevents decompression rock melting when the velocity of extension is 2.5 mm/yr and 3.5 mm/yr, respectively, in low sedimentation rate simulations (~ 0.01 mm/yr) (Fig. 9). Around these thresholds, the magmatic behavior of the system may be influenced solely by the effects of surface processes (Fig. 9B, C). Sedimentation seems also to affect the timing of breakup (Fig. 8C, D). A delay of ~1 to 6 Myr is observed with less efficient surface processes and sediment starvation in the basin, which reduces flexure and subsidence. A thicker sedimentary wedge can mechanically weaken the brittle crust, thereby promoting early crustal rupturing (Fig. 8).

4.2. Model limitations

In this study, numerical models are focused on matching geological constraints such as the total extension, the ultra-slow extension velocity, and the timing of decompression mantle melting. A bi-dimensional setup is used to easily compare the effect of multiple parameters on rift evolution since inception of lithospheric necking to breakup and following oceanization. Obviously, our 2-D models cannot capture the natural complexity of the entire West Antarctic Rift System, which underwent at least a phase of Cretaceous diffuse extension and migration of the extension locus in the Cenozoic. Limitations arise from (1) the impossibility to account for strike-parallel rifting dynamics, particularly disregarding the strike-slip strain in WRS (Granot and Dyment, 2018; Sauli et al., 2021), (2) the presence of inherited structures and juxtaposition of tectonic units (Tinto et al., 2019; Olivetti et al., 2023) which may have conditioned rift basins architecture (Perron et al., 2021).

Surface processes are modeled by a diffusion law which approximates the source-to-sink system between the TAM front and the WRS basins, with surface processes efficiency assumed to be time-independent. Sediment transport along the rift axis (e.g., Jourdon et al., 2018) is not included in simulations. However, in the natural system considered, along-rift sediment transport is thought to be negligible, as fluvio-glacial sediment transport and deposition is mostly orthogonal to the rift axis.

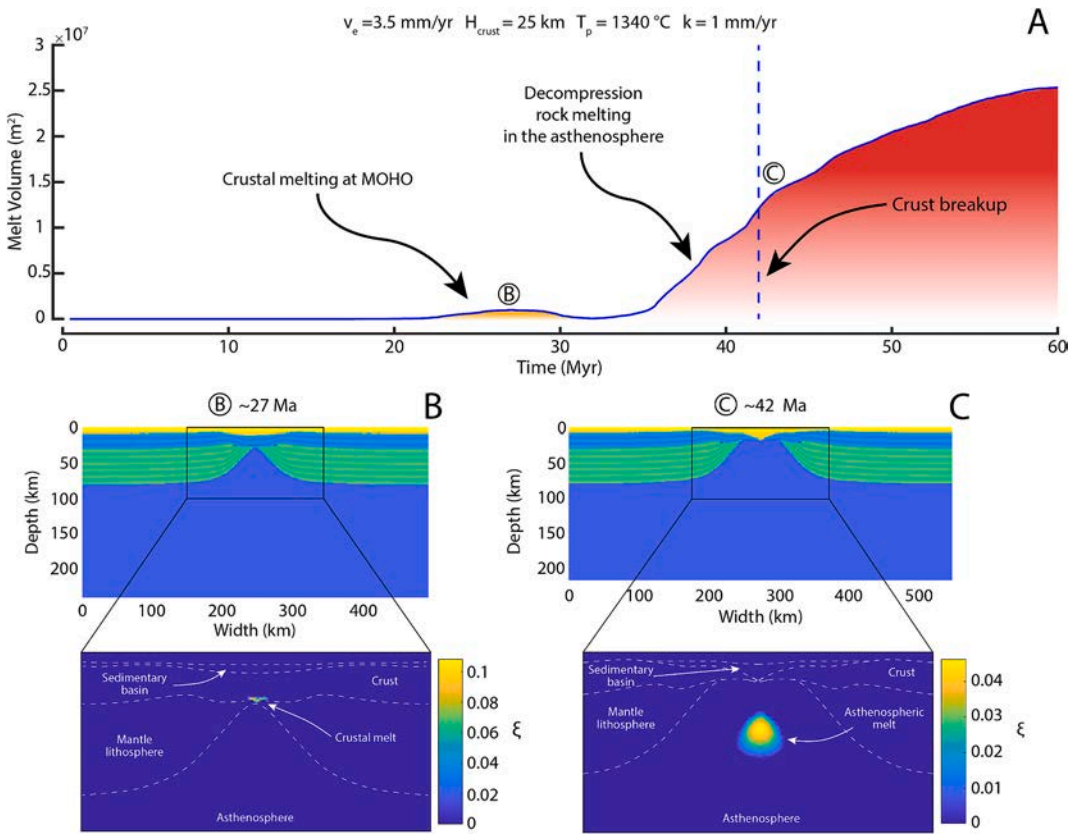

Fig. 5. Tectono-magmatic evolution of the reference model. (A) The graph shows melt volume variation generated by crustal melting and decompression melting during the 60 Myr-long rift simulation. At ~27 Myr (B) and ~ 42 Myr (C), snapshots representing lithologies distribution and the amount of molten material are shown. Dotted line in the graph represents the time at which the breakup of the lithosphere occurred.

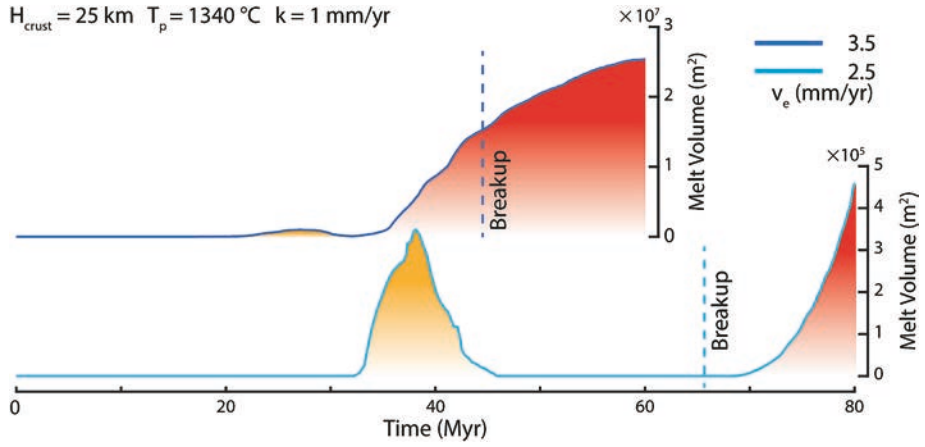

Fig. 6. Results of the parametric study showing timing and volume of crustal (orange-colored) and asthenospheric (red-colored) melting for different extension velocities. Dotted lines indicate lithospheric breakup. It is noted that different scales for the melt volume have been used. (For interpretation of the references to colour in this figure legend, the reader is referred to the web version of this article.)

Partial melting of crustal and asthenospheric material is treated solely as rock melting proportional to temperature in the range between lithology-specific solidus and liquidus curve defined in the setup (Table 1). Fluid-assisted rock melting and migration of melts to the surface are neglected for the sake of simplicity, as previously done by other studies (e.g., Bowling and Harry, 2001; van Wijk et al., 2001; Schmeling, 2010).

5. Discussion

The aridification of Antarctica began during the Middle Miocene Climate Transition (Cramer et al., 2009; Levy et al., 2019; Verret et al., 2023), marking a shift from warmer and wetter (the Middle Miocene Climate Optimum) to colder and drier conditions (Fig. 3B). This transition led to extinction of the tundra biota and a significant decrease of erosion in the Victoria Lands (e.g., Lewis et al., 2008). Geomorphic evidence for low erosion rates following the Middle Miocene Climate Transition are reported in many locations along the Victoria Lands, also

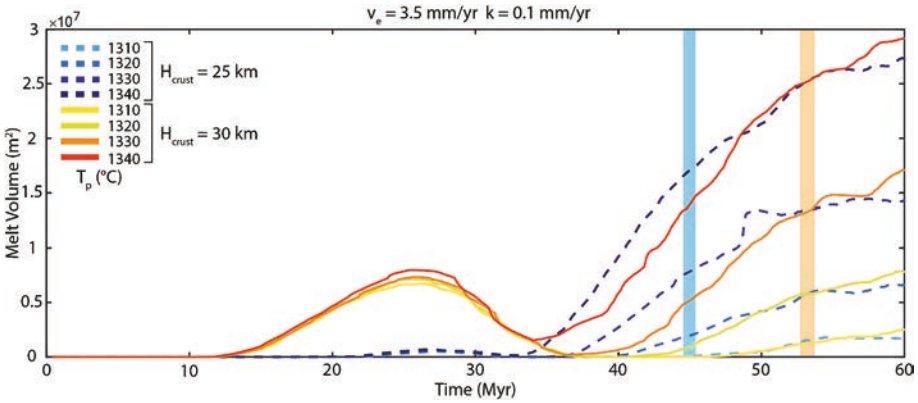

Fig. 7. Results of the parametric study showing timing and volume of melts for a set of different mantle potential temperatures and crust thicknesses. Light blue and orange vertical rectangles indicate the time of breakup for 35 km- and 40 km-thick crust runs. (For interpretation of the references to colour in this figure legend, the reader is referred to the web version of this article.)

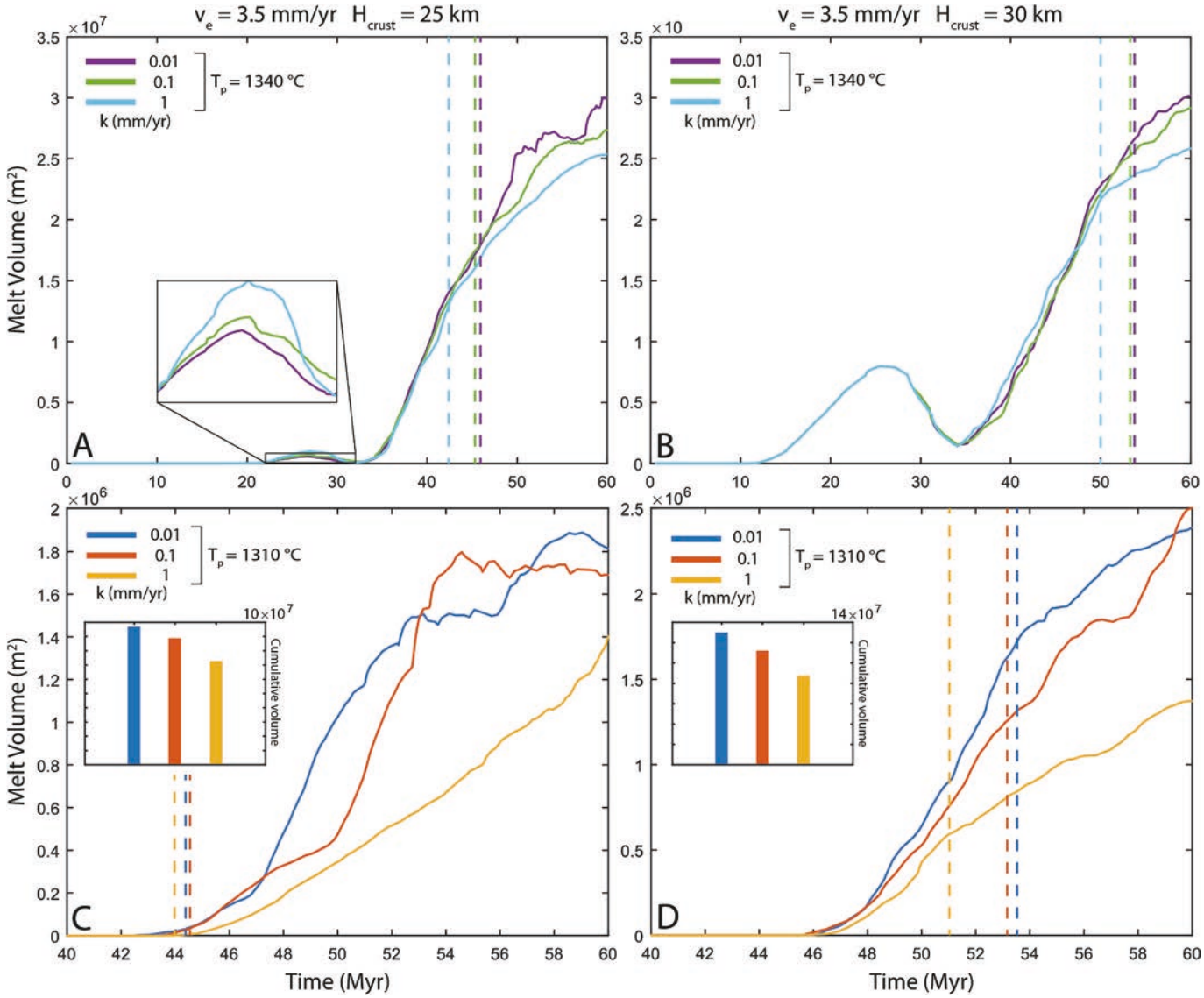

Fig. 8. Results of the parametric study showing timing and volume of melts for a set of different crust thicknesses and surface process efficiencies and mantle potential temperatures. (A) and (C) display melt volumes for an initial crust 25 km-thick; (B) and (D) display melt volumes for an initial crust 30 km-thick. Dotted lines refer to crust breakup inception for different temperatures and surface processes efficiency. Panels in (B) and (D) show the cumulative volumes produced since decompression.

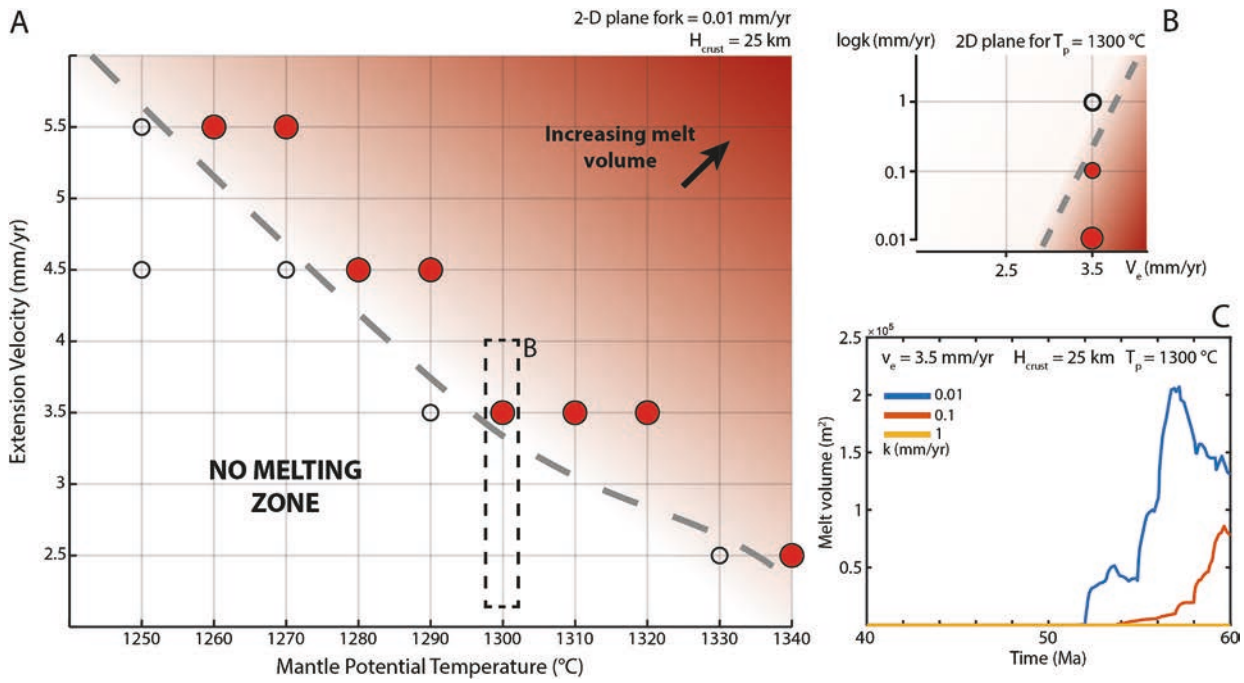

Fig. 9. (A) A representation of asthenospheric melt occurrence dependance by extension velocity and mantle potential temperature. The crust thickness is fixed at 25 km. The red-filled points refer to the occurrence of decompression melting, the hollow points refer to no-melting condition. (B) Melting dependance by surface processes efficiency at constant mantle potential temperature and extension velocity. (C) Time/melt volume relationship of simulations displayed in panel (B). (For interpretation of the references to colour in this figure legend, the reader is referred to the web version of this article.)

confirmed by preservation of dated surfaces ~14 Ma old (Spector and Balco, 2021, and references therein). The sedimentation rate history in the WRS basins (Fig. 3A) depicts, therefore, a strong correlation between climate cooling and the response of the erosional/depositional system.

The onset of volcanism and magmatism in the WRS sector occurred in two distinct phases: the Meander Intrusive Complex (~ 48 to 23 Ma) and the McMurdo Volcanic Group (~ 15 Ma to present) (Fig. 3). Meander Intrusive rocks originated from Eocene decompression of lithospheric domains enriched by very-small-degree partial melting, associated with the Cretaceous wide rifting (Rocchi and Smellie, 2021). For this reason, Eocene to Miocene magmatism in northern Victoria Land would be modeled only considering the ~100 Myr West Antarctic Rift System mantle evolution. Magmatic emplacement was controlled by an intracontinental transfer zone accommodating extension between the Northern Basin and the Victoria Land Basin and Eocene strike-slip tectonic (Salvini et al., 1997; Ferraccioli et al., 2008). Plutons are limited (Fig. 2B), and it is difficult to reconcile their spatial distribution with magmatism governed by lithospheric necking along the entire WRS.

After an amagmatic phase of ~10 Myr, well-developed narrow rifting in the WRS region involves the generation of increasing volumes of melts (Fig. 3C). Prior to 14 Ma, only minor occurrences of volcanics have been recorded in few outcrops along the TAM front (e.g., Mount Morning) (Fig. 8D) (Armienti and Baroni, 1999; Panter and Martin, 2021; Smellie and Martin, 2021; Smellie and Rocchi, 2021) and in offshore cores (McIntosh, 1998). Major volcanoes are superimposed over termination of young tectonic structures, such as the Terror Rift (Miocene to present), as suggested by deformation on volcanoclastic deposits (e.g., Vignaroli et al., 2015). The McMurdo Volcanic Group is interpreted as a magmatic province emplaced as proto-seaward-dipping reflectors (sensu Mutter et al., 1982; Menzies et al., 2002) in an aborted continental rift (Rocchi and Smellie, 2021) due to a change in plate motion (Granot and Dyment, 2018).

Our numerical models indicate that ultra-slow rifting can generate a variable volume of magmas depending on the quantity of sediments delivered into the basin, somewhat similarly to fast rift systems (e.g., Sternai, 2020; Stüwe et al., 2022). Conditions under which such relationship finds expression are: (1) mantle potential temperature equal or higher than 1300 °C, (2) ultra-slow extension velocity and (3) sedimentation rates in the range between 0.01 and 1 mm/yr, conditions that match well the geodynamics of the WRS. It is therefore suggested that the large amount of Paleogene and early Miocene sediments deposited into the rift basins inhibited partial decompression mantle melting, whereas post-Middle Miocene Climate Transition sediment starvation contributed to enhance the regional magmatism (Fig. 10). Inhibition of decompression melting due to sediment loading occurs more efficiently when the crust is very thin. Consistently, WRS basins show an average sedimentary sequence thickness of ~4–5 km, with maximum values of ~10–14 km, similar to or greater than crustal thicknesses which are estimated between 5 and 20 Km (Busetti et al., 1999).

Our modeling suggests that high mantle potential temperatures and a highly stretched crust are the primary favorable conditions for a strong coupling between surface processes and magmatism in ultra-slow rift systems. For the conditions explored here, mantle potential temperatures above 1300 °C are required to enable variable sediment loads to foster or inhibit mantle melting (Fig. 9). Mantle potential temperatures between 1300 °C and 1340 °C are moderately hotter than normal subcontinental T_p, commonly around ~1200–1250 °C (e.g., Reston and Morgan, 2004). Perinelli et al. (2006) constrain T_p of near-primary melts in McMurdo Group alkali volcanic in the range between 1250 and 1350 °C using geothermometric data from peridotite xenoliths. Our models suggest that a mantle potential temperature between 1250 and 1300 °C requires extension velocities >3.5 mm/yr to generate asthenospheric melts (Fig. 9A). It is also noteworthy that around the limit between melting and no-melting (Fig. 9A), the magma-generation threshold may be modulated by modifying the sedimentation rates (Fig. 9B-C). Hot temperatures at the lithosphere-asthenosphere boundary may be a consequence of the multi-stage evolution of the West Antarctic Rift System, so that warm, narrow rifting in WRS is a result of the Cretaceous to Paleogene wide rifting phase (Huerta and Harry, 2007). Another possible contribution to relatively high mantle temperatures, however, could be upwelling due to regional mantle flow at the

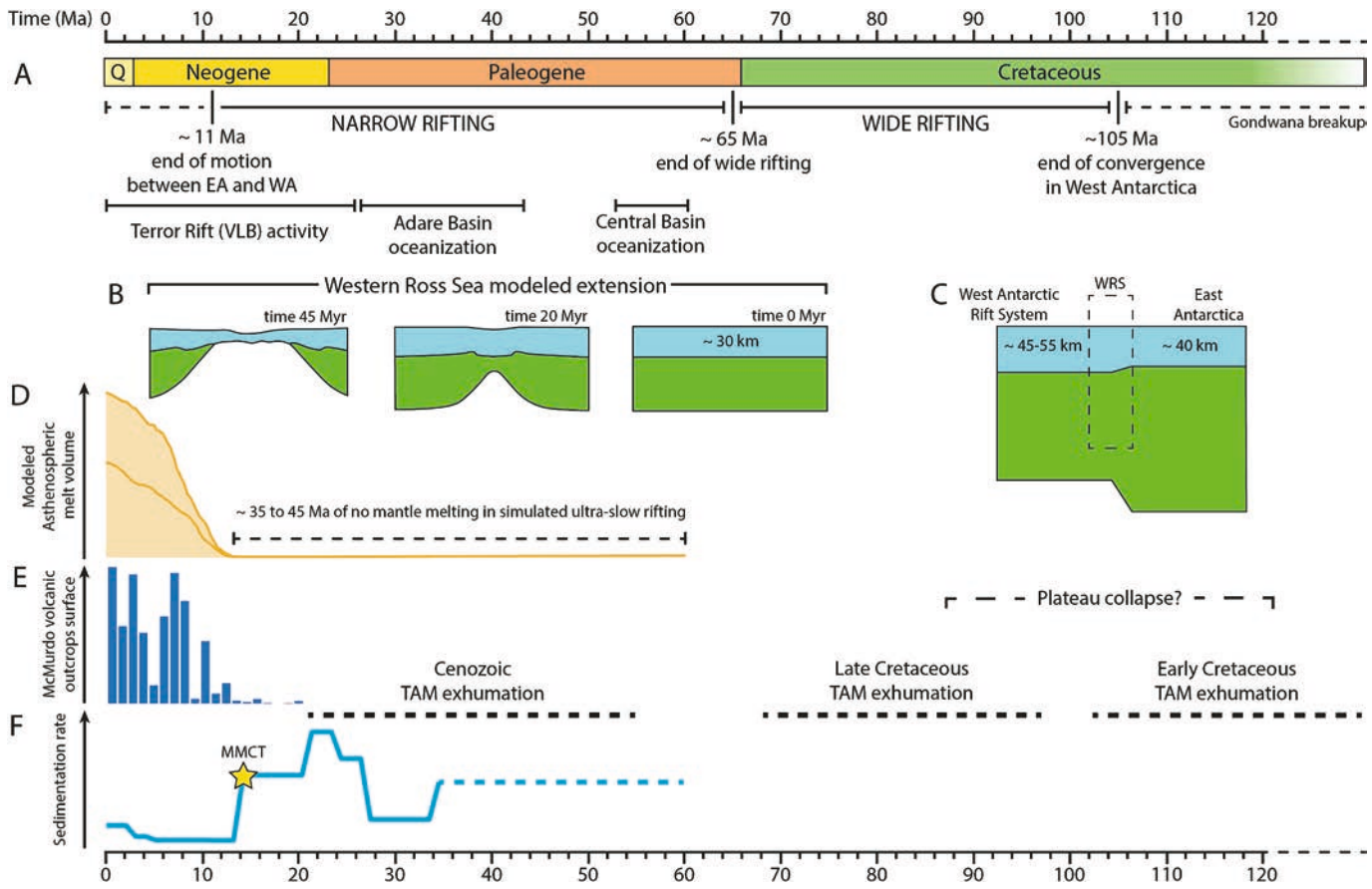

Fig. 10. (A) Chronological chart of West Antarctic Rift System evolution since Cretaceous (Huerta and Harry, 2007; Davey et al., 2016; Granot and Dyment, 2018; Sauli et al., 2021). (B) Depth-dependent narrow rifting as described by our models. (C) The initial setup for the wide rifting from Huerta and Harry (2007), the WRS is at the transition with the East Antarctica cratonic lithosphere. The colored domains refer to the crust (aquamarine) and mantle lithosphere (green). (D) Mantle melting from Fig. 8D. (E) Time/area distribution of volcanic rock from Fig. 3D. (F) Sedimentation rate oscillation from Fig. 3A. Abbreviations: Q, Quaternary; EA, East Antarctica; WA West Antarctica; VLB, Victoria Land Basin; MMCT Middle Miocene Climate Transition. Timing for TAM exhumation from Fitzgerald (2002). (For interpretation of the references to colour in this figure legend, the reader is referred to the web version of this article.)

boundary with the craton since the Eocene (Faccenna et al., 2008; Panter et al., 2018).

An average 3.5 mm/yr velocity is consistent with: first, the onset of mantle-sourced magmatism across the WRS region after at least ~35 Myr of amagmatic rifting (Fig. 10C), and second, the basins width. Conversely, the Adare Basin shows the presence of oceanic crust at its center, formed following rapid seafloor spreading between 43 and 26 Ma. If Adare Basin extension started around 60–65 Ma at ~10 mm/yr, the thinned crust would have completely broken after <20 Myr (Cande et al., 2000). Overall, the timing of this breakup is consistent with similar modeling performed at 10 mm/yr (Sternai, 2020). Although spreading rates may have changed along the Cenozoic evolution of the WRS, a constant extension velocity facilitates the comparison with other natural systems. Additionally, considering that the magmatic (Fig. 3C-D) and depositional history (Fig. 3A) are similar for all WRS basins, results presented here may well represent the overall regional-scale geodynamic evolution. Under these assumptions adopted here, the upper range of mantle potential temperatures proposed by Perinelli et al. (2006) is suitable for the study area.

Surface processes active on a highly stretched crust are more effectively able to modulate decompression melting, since the thermomechanical effects of sediments are transmitted to greater depths. The stretching factor of the West Antarctic Rift System is estimated on average as greater than ~2 (Wilson and Luyendyk, 2009; Tankersley et al., 2022), and nearly ~6 for the WRS region (Wilson and Luyendyk, 2009), coherently with a thinned crust of ~5–10 km in Victoria Land Basin (Busetti et al., 1999). We speculate that, in the middle Miocene, the crust was stretched to at least a stretching factor of 5, considering that minor horizontal extension occurred since that time (Granot and Dyment, 2018; Sauli et al., 2021). The West Antarctic crust, thickened to ~45–55 km (Fig. 10B) (Bialas et al., 2007; Huerta and Harry, 2007; Harry et al., 2018) due to Paleozoic to Early Cretaceous convergence, was affected by wide rifting in Late Cretaceous (~ 105 Ma). Simulations with an initial crustal thickness of ~30 km (e.g., Fig. 8D) at the wide-to-narrow rifting transition (i.e., ~ 60–65 Ma) (Fig. 10A) match the magmatic evolution. If the crustal thickness at the time of the wide-to-narrow rifting transition was thinner, it would have ruptured even in an ultra-slow extension scenario. The modulation of magmatism exerted by sediment loading occurs during relatively late rifting stages but prior to oceanization, when the crust is already highly stretched (Fig. 8D).

In addition to asthenospheric melting, our models suggest that some crustal melts can be generated a few tens of millions of years before the crustal breakup. Initial crustal melts forming at the Moho are generated by heating due to rising hot asthenospheric material, in combination to thermal blanketing due to sediment deposition into the rift basin, as also suggested by previous studies (Stephenson et al., 1989; Burov and Cloetingh, 1997; Buiter et al., 2008). Crustal partial melting occurs near the Moho and may generate a wide spectrum of magmatic products (Viereck, 1988; Gans, 1989; Schenker et al., 2012). We suggest that melts may laterally migrate exploiting lower crust ductile flow (Burov and Cloetingh, 1997), nevertheless this remains unconstrained by field data and is an open field of study (Cloetingh et al., 2023; Sternai, 2023).

Crustal melting at Moho levels and crustal underplating may also help thickening the crust beneath the TAM and contribute to uplift of the rift shoulders by isostasy, similarly to thermal buoyancy compensation as suggested in literature (e.g., ten Brink et al., 1997; Brenn et al., 2017).

A secondary effect of surface processes observed in numerical simulations is the modulation of the timing of continental breakup, which may be delayed by ~1–5 Myr (depending on the crustal thickness, mantle potential temperature and extension velocity) when the imposed sedimentation rate is low. In models run by Sternai (2020), which account for extension rate of 10 mm/yr and relatively low mantle potential temperatures (1200–1250 °C), the breakup is delayed by about 2–3 Myr when the sedimentation rate is high. This behavior is related to thermal blanketing and flexural stresses that weaken the upper lithosphere contributing to advantage viscous over brittle deformation and thus promoting stretching (Burov and Cloetingh, 1997; Sternai, 2020). Conversely, in ultra-slow rifts the asthenospheric material has enough time to cool down and strengthen during upwelling regardless of the high initial mantle potential temperature. High sedimentary loading thus fosters flexural brittle deformation anticipating the breakup. The decrease of sedimentation rates in the WRS region may inhibit the brittle strain related to flexure and promote the stretching phase before the onset of oceanization.

6. Conclusion

Numerical experiments suggest that the amount of asthenospheric melts in ultra-slow continental rifts with a 30 km thick initial crust and mantle potential temperatures higher than 1300 °C may be conditioned by the regional erosion/sedimentation rates. These conditions apply to the western Ross Sea basins and Transantarctic Mountains coast, where a wide alkali province was emplaced in the middle Miocene, synchronous to global climate cooling as well as regional aridification and sediment starvation in the rift basins. The synchronicity between the onset of magmatism and reduced sedimentation rates in absence of major tectonic changes points to surface processes as a leading factor behind the McMurdo Group alkali volcanic activity. Overall, a load-controlled modulation on partial mantle melting is possible in ultra-slow continental rifts even before the breakup stage, when the extended lithosphere has been stretching for tens of Myr. In the Ross Sea, middle Miocene climate aridification and decreasing sedimentation rates could have extended the stretching phase prior to complete crustal rupturing.

CRediT authorship contribution statement

Marco Fioraso: Writing – review & editing, Writing – original draft, Visualization, Methodology, Investigation, Formal analysis, Data curation, Conceptualization. **Pietro Sternai:** Writing – review & editing, Writing – original draft, Software, Methodology, Investigation, Conceptualization. **Valerio Olivetti:** Writing – review & editing, Writing – original draft, Supervision, Conceptualization. **Maria Laura Balestrieri:** Writing – review & editing, Conceptualization. **Massimiliano Zattin:** Writing – review & editing, Conceptualization. **Gianluca Cornamusini:** Writing – review & editing, Supervision.

Declaration of competing interest

The authors declare that they have no known competing financial interests or personal relationships that could have appeared to influence the work reported in this paper.

Data availability

Data will be made available on request.

Acknowledgments

We would like to thank the Editor, Liviu Matenco; Zoltán Erdős and two anonymous reviewers for their thoughtful reviews which positively contribute to improve the manuscript. VO and MZ were supported by Geosciences Department funding (BIRD_182501). PS has been supported by Fondazione Cariplo and Fondazione CDP (Grant n° 2022- 1546_001), by the Italian Ministry of Education, MUR (Project Dipartimenti di Eccellenza, TECLA, Department of Earth and Environmental Sciences, University of Milano-Bicocca) and by the Alexander von Humbolt Foundation.

References

Armienti, P., Baroni, C., 1999. Cenozoic climatic change in Antarctica recorded by volcanic activity and landscape evolution. Geology 27, 617–620. https://doi.org/10.1130/0091-7613(1999)027<0617:CCCIAR>2.3.CO;2.

Balestrieri, M.L., Olivetti, V., Rossetti, F., Gautheron, C., Cattò, S., Zattin, M., 2020. Topography, structural and exhumation history of the Admiralty Mountains region, northern Victoria Land. Antarctica. Geoscience Frontiers 1841–1858. https://doi.org/10.1016/j.gsf.2020.01.018.

Barr, I.D., Spagnolo, M., Rea, B.R., et al., 2022. 60 million years of glaciation in the Transantarctic Mountains. Nat. Commun. 13, 5526. https://doi.org/10.1038/s41467-022-33310-z.

Bialas, R.W., Buck, W.R., 2009. How sediment promotes narrow rifting: Application to the Gulf of California. Tectonics 28. https://doi.org/10.1029/2008TC002394.

Bialas, R.W., Buck, W.R., Studinger, M., Fitzgerald, P., 2007. Plateau collapse model for the Transantarctic Mountains-West Antarctic Rift System: Insights from numerical experiments. Geology 35, 687–690. https://doi.org/10.1130/G23825A.1.

Bowling, J.C., Harry, D.L., 2001. Geodynamic models of continental extension and the formation of non-volcanic rifted continental margins. In: Wilson, R.C.L., Whitmarsh, R.B., Taylor, B., Froitzheim, N. (Eds.), Non-Volcanic Rifting Of Continental Margins: A Comparison Of Evidence From Land And Sea, vol. 187. Geol. Soc. Lond. Special Pubb, pp. 511–536. https://doi.org/10.1144/GSL.SP.2001.187.01.25.

Brenn, G.R., Hansen, S.E., Park, Y., 2017. Variable thermal loading and flexural uplift along the Transantarctic Mountains, Antarctica. Geology 45, 463–466. https://doi.org/10.1130/G38784.1.

Brun, J.P., Buck, R., Mcclay, K., Kusznir, N., Louden, K.E., Mckenzie, D., 1999. Narrow Rifts Versus Wide Rifts: Inferences for the Mechanics of Rifting from Laboratory experiments [and Discussion]. Phil. Trans. R. Soc. Lond. 357, 695–712. https://www.jstor.org/stable/55066.

Brune, S., Corti, G., Ranalli, G., 2017. Controls of inherited lithospheric heterogeneity on rift linkage: Numerical and analog models of interaction between the Kenyan and Ethiopian rifts across the Turkana depression. Tectonics 36, 1767–1786. https://doi.org/10.1002/2017TC004739.

Brune, S., Kalawole, F., Olive, J.A., Stamps, D.S., Buck, W.R., Buiter, S.J.H., Furman, T., Shillington, D.J., 2023. Geodynamics of Continental Rift Initiation and Evolution. Nat. Rev. Earth Environ. https://doi.org/10.1038/s43017-023-00391-3.

Buck, W.R., 1991. Modes of continental lithospheric extension. J. Geophys. Res. 96 (B12) https://doi.org/10.1029/91JB01485.

Buiter, S.J.H., Huismans, R.S., Beaumont, C., 2008. Dissipation analysis as a guide to mode selection during crustal extension and implications for the styles of sedimentary basins. J. Geophys. Res. 113 (B06406) https://doi.org/10.1029/2007JB005272.

Burov, E., Cloetingh, S., 1997. Erosion and rift dynamics: new thermomechanical post-rift evolution of extensional basins. Earth Planet. Sci. Lett. 150, 7–26. https://doi.org/10.1016/S0012-821X(97)00069-1.

Burov, E., Poliakov, A., 2001. Erosion and rheology controls on synrift and postrift evolution: Verifying old and new ideas using a fully coupled numerical model. J. Geophys. Res. Solid Earth 106, 16461–16481. https://doi.org/10.1029/2001jb000433.

Busetti, M., Spadini, G., Van der Wateren, F.M., Cloetingh, S., Zanolla, C., 1999. Kinematic modelling of the West Antarctic Rift System, Ross Sea, Antarctica. Glob. Planet. Change 23, 79–103. https://doi.org/10.1016/S0921-8181(99)00052-1.

Cande, S.C., Stock, J.M., Dietmar Muller, R., Ishihara, T., 2000. Cenozoic motion between East and West Antarctica. Nature 404, 145–150. https://doi.org/10.1038/35004501.

Cloetingh, S., Sternai, P., Koptev, A., Ehlers, T.A., Gerya, T., Kovács, I., Oerlemans, J., Beekman, F., Lavallée, Y., Dingwell, D., Békési, E., Porkolàb, K., Tesauro, M., Lavecchia, A., Botsyun, S., Muller, V., Roure, F., Serpelloni, E., Matenco, L., Castelltort, S., Giovannelli, D., Brovarone, A.V., Malaspina, N., Coletti, G., Valla, P., Limberger, J., 2023. Coupled surface to deep Earth processes: Perspectives from TOPO-EUROPE with an emphasis on climate- and energy-related societal challenges. Glob. Planet. Change 226, 104140. https://doi.org/10.1016/j.gloplacha.2023.104140.

Cooper, A.K., Davey, F.J., Behrendt, J.C., 1991. Structural and depositional controls on Cenozoic and (?) Mesozoic strata beneath the western Ross Sea. In: Thomson, M.R.A., Crame, J.A., Thomson, J.W. (Eds.), Geological Evolution of Antarctica. Cambridge University Press, Cambridge, pp. 279–283.

Courant, R., 1928. On the partial difference equations of mathematical physics. Math. Ann. 100, 32–74.

Cramer, B.S., Toggweiler, J.R., Wright, J.D., Katz, M.E., Miller, K.G., 2009. Ocean overturning since the late cretaceous: Inferences from a new benthic foraminiferal isotope compilation. Paleoceanography 24. https://doi.org/10.1029/2008PA001683.

Davey, F.J., De Santis, L., 2006. A multi-phase rifting model for the Victoria Land Basin, Western Ross Sea. In: Fütterer, D.K., Damaske, D., Kleinschimdt, G., Miller, H., Tessensohn, F. (Eds.), Antarctica. Springer, Berlin, Heidelberg. https://doi.org/10.1007/3-540-32934-X_38.

Davey, F.J., Granot, R., Cande, S.C., Stock, J.M., Selvans, M., Ferraccioli, F., 2016. Synchronous oceanic spreading and continental rifting in West Antarctica. Geophys. Res. Lett. 43, 6162–6169. https://doi.org/10.1002/2016GL069087.

Davey, F.J., Cande, S., Stock, J., 2022. Cenozoic continental rifting in the North-Western Ross Sea. N. Z. J. Geol. Geophys. 65, 389–396. https://doi.org/10.1080/00288306.2021.1891942.

Dick, H.J.B., Lin, J., Schouten, H., 2003. An ultraslow-spreading class of ocean ridge. Nature 426.

Durkin, K., Day, J., Panter, K.S., et al., 2023. Petrogenesis of alkaline magmas across a continent to ocean transect, northern Ross Sea. Antarctica. Chemical Geology 641. https://doi.org/10.1016/j.chemgeo.2023.121780.

Faccenna, C., Rossetti, F., Becker, T.W., Danesi, S., Morelli, A., 2008. Recent extension driven by mantle upwelling beneath the Admiralty Mountains (East Antarctica). Tectonics 27. https://doi.org/10.1029/2007TC002197.

Ferraccioli, F., Armadillo, E., Zunino, A., Bozzo, E., Rocchi, S., Armienti, P., 2008. Magmatic and tectonic patterns over the Northern Victoria Land sector of the Transantarctic Mountains from new aeromagnetic imaging. Tectonophysics 478, 43–61. https://doi.org/10.1016/j.tecto.2008.11.028.

Fitzgerald, P., 2002. Tectonics and landscape evolution of the Antarctic plate since the breakup of Gondwana, with an emphasis on the West Antarctic Rift System and the Transantarctic Mountains. In: Gamble, J.A., John, A., Skinner, D.N.B., David, N.B., Henrys, S. (Eds.), Antarctica at the Close of a Millennium, 35. R. Soc. N. Z. Bull, pp. 453–469.

Fitzgerald, P., Baldwin, S.L., 1997. Detachment fault model for the evolution of the Ross Embayment. In: Ricci, C.A. (Ed.), The Antarctic Region: Geological Evolution and Processes. Terra Antarctica Publication, Siena.

Fitzgerald, P.G., Goodge, J.W., 2022. Exhumation and tectonic history of inaccessible subglacial interior East Antarctica from thermochronology on glacial erratics. Nat. Commun. 13, 6217. https://doi.org/10.1038/s41467-022-33791-y.

Gans, P.B., 1989. Synextensional Magmatism in the Basin and Range Province: A Case Study from the Eastern Great Basin. Geol. Soc. Am. Spec 233.

Gerya, T., 2019. Introduction to Numerical Geodynamic Modelling. Second edition. Cambridge University Press. https://doi.org/10.1017/9781316534243.

Gerya, T.V., Yuen, D.A., 2003. Characteristics-based marker-in-cell method with conservative finite-differences schemes for modeling geological flows with strongly variable transport properties. Phys. Earth Planet. In. 140, 293–318. https://doi.org/10.1016/j.pepi.2003.09.006.

Gerya, T.V., Yuen, D.A., 2007. Robust characteristics method for modeling multiphase visco-elasto-plastic thermo-mechanical problems. Phys. Earth Planet. In. 163, 83–105. https://doi.org/10.1016/j.pepi.2007.04.015.

Goodge, J.W., 2020. Geological and tectonic evolution of the Transantarctic Mountains, from ancient craton to recent enigma. Gondw. Res. 80, 50–122. https://doi.org/10.1016/j.gr.2019.11.001.

Granot, R., Dyment, J., 2018. Late Cenozoic unification of East and West Antarctica. Nat. Commun. 9, 3189. https://doi.org/10.1038/s41467-018-05270-w.

Harry, D.L., Jourdan, L.A., Sumant, J., 2018. Geodynamic models of the West Antarctic Rift System: Implications for the mantle thermal state. Geosphere 14. https://doi.org/10.1130/GES01594.1.

Hochmuth, K., Gohl, K., Leitchenkov, G.L., Sauermilch, I., Whittaker, J., Uenzelmann-Neben, G., Davy, B., DeSantis, L., 2020. Paleobathymetry and sediment thickness of the Southern Ocean since 34 Ma. Pangaea. https://doi.org/10.1594/PANGAEA.918663.

Huerta, A.D., Harry, D.L., 2007. The transition from diffuse to focused extension: Modeled evolution of the West Antarctic Rift system. Earth Planet. Sci. Lett. 255, 133–147. https://doi.org/10.1016/j.epsl.2006.12.011.

Huybers, P., Langmuir, C., 2009. Feedback between deglaciation, volcanism, and atmospheric CO2, Earth Planet. Sci. Lett. 286, 479–491. https://doi.org/10.1016/j.epsl.2009.07.014.

Jordan, T.A., Riley, T.R., Siddoway, C.S., 2020. The geological history and evolution of West Antarctica. Nat Rev Earth Environ 1, 117–133. https://doi.org/10.1038/s43017-019-0013-6.

Jourdon, A., Le Pourhiet, L., Petit, C., Rolland, Y., 2018. Impact of range-parallel sediment transport on 2D thermo-mechanical models of mountain belts: Application to the Kyrgyz Tien Shan. Terra Nova 30, 279–288. https://doi.org/10.1111/ter.12337.

Jull, M., McKenzie, D., 1996. The effect of deglaciation on mantle melting beneath Iceland. J. Geophys. Res. 101, 21815–21828. https://doi.org/10.1029/96JB01308.

Koptev, A., Burov, E., Gerya, T., Le Pourhiet, L., Leroy, S., Calais, E., Jolivet, L., 2018. Plume-induced continental rifting and break-up in ultra-slow extension context: Insights from 3D numerical modeling. Tectonophyisics 746. https://doi.org/10.1016/j.tecto.2017.03.025.

Kyle, P.R., 1990a. McMurdo Volcanic Group Western Ross Embayment: Introduction. In: LeMasurier, W., Thomson, J. (Eds.), In: "Volcanism of the Antarctic Plate and Southern Oceans", vol. 48. American Geophysical Union, pp. 18–25. Antarctic Research Series,.

Kyle, P.R., 1990b. Melbourne Volcanic Province: Summary. In: LeMasurier, W., Thomson, J. (Eds.), In: "Volcanism of the Antarctic Plate and Southern Oceans", vol. 48. American Geophysical Union, pp. 48–52. Antarctic Research Series,.

Levy, R., Harwood, D., Florindo, F., Sangiorgi, F., Tripati, R., von Eynatten, H., Gasson, E., Kuhn, G., Tripati, A., DeConto, R., Fielding, C., Field, B., Golledge, N., McKay, R., Naish, T., Olney, M., Pollard, D., Schouten, S., Talarico, F., Warny, S., Willmott, V., Acton, G., Panter, K., Paulsen, T., Taviani, M., SMS Science Team, 2016. Antarctic ice sheet sensitivity to atmospheric CO_2 variations in the early to mid-Miocene. Pnas. https://doi.org/10.1073/pnas.1516030113.

Levy, R.H., Meyers, S.R., Naish, T.R., Golledge, N.R., McKay, R.M., Crampton, J.S., DeConto, R.M., De Santis, L., Florindo, F., Gasson, E.G.W., Hardwood, D.M., Luyendyk, B.P., Powell, R.D., Clowes, C., Kulhanek, D.K., 2019. Antarctic ice-sheet sensitivity to obliquity forcing enhanced through ocean connections. Nat. Geosci. 12, 132–137. https://doi.org/10.1038/s41561-018-0284-4.

Lewis, A.R., Marchant, D.R., Ashworth, A.C., Hedenä, S.E.L., Hemming, S.R., Johnson, J. V., Leng, M.J., Machlus, M.L., Newton, A.E., Raine, J.I., Willenbring, J.K., Williams, M., Wolfe, A.P., 2008. Mid-Miocene cooling and the extinction of tundra in continental Antarctica. Proc. Nat. Acad. Sci. 105, 10676–10680. https://doi.org/10.1073/pnas.0802501105.

Lindeque, A., Gohl, K., Wobbe, F., Uenzelmann-Neben, G., 2016. Preglacial to glacial sediment thickness grids for the Southern Pacific margin of West Antarctica. Geochem. Geophys. Geosystems 17, 4276–4285. https://doi.org/10.1002/2016GC006401.

Martin, A.P., Cooper, A.F., Price, R.C., Kyle, P.R., Gamble, J.A., 2021. Erebus Volcanic Province: Petrology. In: Smellie, J.L., Panter, K.S., Geyer, A. (Eds.), Volcanism in Antarctica: 200 Million Years of Subduction, Rifting and Continental Break-up. Geol. Soc. Lond. Memoirs. https://doi.org/10.1144/M55-2018-80

McIntosh, W.C., 1998. $^{40}Ar/^{39}Ar$ geochronology of volcanic clasts and pumice in CRP-1 core, Cape Roberts. Antarctica. Terra Antarct. 5, 683–690.

McIntosh, W.C., Kyle, P.R., 1990. Hallett Volcanic Province: Summary. In: LeMasurier, W., Thomson, J. (Eds.), In: "Volcanism of the Antarctic Plate and Southern Oceans", 48. American Geophysical Union, pp. 26–31. Antarctic Research Series,.

McKay, R.M., Escutia, C., De Santis, L., Donda, F., Duncan, B., Gohl, K., Gulick, S., Hernández-Molina, J., Hillenbrand, C.D., Hochmuth, K., Kim, S., Kuhn, G., Larter, R., Leitchenkov, G.H., Levy, R.R., Naish, T., O'Brien, P.F., Pérez, L.E., Shevenell, A., Williams, T., 2022. Cenozoic history of Antarctic glaciation and climate from onshore and offshore studies. In: Florindo, F., Siegert, M., De Santis, L., Naish, T. (Eds.), Antarctic Climate Evolution. Elsevier, pp. 41–164. https://doi.org/10.1016/b978-0-12-819109-5.00008-6.

McKenzie, D., Bickle, M.J., 1988. The volume and Composition of Melt Generated by Extension of the Lithosphere. J. Petrol. 29, 625–679. https://doi.org/10.1093/petrology/29.3.625.

Menzies, M.A., Klemperer, S.L., Ebinger, C.J., Baker, J., 2002. Characteristics of volcanic rifted margins. In: Menzies, M.A., Klemperer, S.L., Ebinger, C.J., Baker, J. (Eds.), Volcanic Rifted Margins, 362. Geol. Soc. Am. Spec. Pap., pp. 1–14

Morlighem, M., Rignot, E., Binder, T., Blankenship, D., Drews, R., Eagles, G., Eisen, O., Ferraccioli, F., Forsberg, R., Fretwell, P., Goel, V., Greenbaum, J.S., Gudmundsson, H., Guo, J., Helm, V., Hofstede, C., Howat, I., Humbert, A., Jokat, W., Karlsson, N.B., Lee, W.S., Matsuoka, K., Millan, R., Mouginot, J., Paden, J., Pattyn, F., Roberts, J., Rosier, S., Ruppel, A., Seroussi, H., Smith, E.C., Steinhage, D., Sun, B., Broeke, M.R., van den Ommen, T.D., van Wessem, M., van Young, D.A., 2020. Deep glacial troughs and stabilizing ridges unveiled beneath the margins of the Antarctic ice sheet. Nat. Geosci. 13, 132–137. https://doi.org/10.1038/s41561-019-0510-8.

Mutter, J.C., Talwani, M., Stoffa, P.L., 1982. Origin of seaward-dipping reflectors in oceanic crust off the Norwegian margin by "subaerial sea-floor spreading". Geology 10, 353–357.

Olivetti, V., Balestrieri, M.L., Rossetti, F., Talarico, F.M., 2013. Tectonic and climatic signals from apatite detrital fission track analysis of the Cape Roberts Project core records, South Victoria Land, Antarctica. Tectonophysics 594, 80–90. https://doi.org/10.1016/j.tecto.2013.03.017.

Olivetti, V., Rossetti, F., Balestrieri, M.L., Pace, D., Cornamusini, G., Talarico, F., 2018. Variability in uplift, exhumation and crustal deformation along the Transantarctic Mountains front in southern Victoria Land, Antarctica. Tectonophysics 745, 229–244. https://doi.org/10.1016/j.tecto.2018.08.017.

Olivetti, V., Balestrieri, M.L., Chew, D., Zurli, L., Zattin, M., Pace, D., Drakou, F., Cornamusini, G., Perotti, M., 2023. Ice volume variations and provenance trends in the Oligocene-early Miocene glaciomarine sediments of the Central Ross Sea, Antarctica (DSDP Site 270). Glob. Planet. Change. https://doi.org/10.1016/j.gloplacha.2023.104042.

Panter, K.S., Martin, A.P., 2021. West Antarctic mantle deduced from mafic magmatism. In: Martin, A.P., van der Wal, W. (Eds.), The Geochemistry and Geophysics of the Antarctic Mantle. Geological Society, London, Memoirs, p. 56.

Panter, K.S., Castillo, P., Krans, S., Deering, C., McIntosh, W., Valley, J.W., Kitajima, K., Kyle, P., Hart, S., Blusztajn, J., 2018. Melt origin across a rifted continental margin: a case for subduction-related metasomatic agents in the lithospheric source of alkaline basalt, NW Ross Sea. Antarctica. J. Petrol. 59, 517–558. https://doi.org/10.1093/petrology/egy036.

Paxman, G.J.G., Jamieson, S.S.R., Hochmuth, K., Gohl, K., Bentley, M.J., Leitchenkov, G., Ferraccioli, F., 2019. Reconstructions of Antarctic topography since the Eocene–Oligocene boundary. Palaeogeogr. Palaeoclimatol. Palaeoecol. 535 https://doi.org/10.1016/j.palaeo.2019.109346.

Perinelli, C., Armienti, P., Dallai, L., 2006. Geochemical and O-isotope constraints on the evolution of lithospheric mantle in the Ross Sea rift area (Antarctica). Contrib. Mineral. Petrol. 151, 245–266. https://doi.org/10.1007/s00410-006-0065-8.

Perron, P., Le Pourhiet, L., Guiraud, M., Vennin, E., Moretti, I., Portier, E., Konaté, M., 2021. Control of inherited accreted lithospheric heterogeneity on the architecture

and the low, long-term subsidence rate of intracratonic basins. Bull. Soc. Géol. Fr. 192 https://doi.org/10.1051/bsgf/2020038.
Reston, T.J., Morgan, J.P., 2004. Continental geotherm and the evolution of rifted margins. Geology 32, 133–136. https://doi.org/10.1130/G19999.1.
Rilling, S., Musaka, S., Wilson, T., Lawver, L., Hall, C., 2009. New determinations of $^{40}Ar/^{39}Ar$ isotopic ages and flow volumes for Cenozoic volcanism in the terror Rift, Ross Sea. Antarctica. J. Geophys. Res. 114 https://doi.org/10.1029/2009JB006303.
Rocchi, S., Smellie, J.L., 2021. Northern Victoria Land: Petrology. In: Smellie, J.L., Panter, K.S., Geyer, A. (Eds.), Volcanism in Antarctica: 200 Million Years of Subduction, Rifting and Continental Break-Up. Geol. Soc. Lond. Memoirs. https://doi.org/10.6084/m9.figshare.c.5198177.
Rocchi, S., Armienti, P., D'Orazio, M., Tonarini, S., Wijbrans, J.R., di Vincenzo, G., 2002. Cenozoic magmatism in the western Ross Embayment: Role of mantle plume versus plate dynamics in the development of the West Antarctic Rift System. J. Geophys. Res. Solid Earth 107. https://doi.org/10.1029/2001jb000515. ECV 5-1-ECV 5-22.
Rossetti, F., Storti, F., Busetti, M., Lisker, F., Di Vincenzo, G., Laufer, A.L., Rocchi, S., Salvini, F., 2006. Eocene initiation of Ross Sea dextral faulting and implications for East Antarctic neotectonics. J. Geol. Soc. Lond. 163, 119–126. https://doi.org/10.1144/0016-764905-005.
Salvini, F., Brancolini, G., Busetti, M., Storti, F., Mazzarini, F., Coren, F., 1997. Cenozoic geodynamics of the Ross Sea region, Antarctica: Crustal extension, intraplate strike-slip faulting, and tectonic inheritance. J. Geophys. Res. 102 (B11), 24669–24696. https://doi.org/10.1029/97JB01643.
Sauli, C., Sorlien, C., Busetti, M., De Santis, L., Geletti, R., Wardell, N., Luyendyk, B.P., 2021. Neogene Development of the terror Rift, Western Ross Sea. Antarctica. Geochem. Geophys. Geosystems 22. https://doi.org/10.1029/2020GC009076.
Schenker, F.L., Gerya, T., Burg, J.P., 2012. Bimodal behavior of extended continental lithosphere: Modeling insight and application to thermal history of migmatitic core complexes. Tectonophysics 579, 88–103. https://doi.org/10.1016/j.tecto.2012.07.002.
Schmeling, H., 2010. Dynamic models of continental rifting with melt generation. Tectonophysics 480, 33–47. https://doi.org/10.1016/j.tecto.2009.09.005.
Siddoway, C.S., 2008. Tectonics of the West Antarctic Rift System: New light on the history and dynamics of distributed intracontinental extension. In: Cooper, A.K., Barrett, P.J., Stagg, H., Storey, E., Wise, W. (Eds.), Proceedings of the 10th International Symposium on Antarctic Earth Sciences. The National Academies Press. https://doi.org/10.3133/of2007-1047.kp09.
Siddoway, C.S., Baldwin, S.L., Fitzgerald, P.G., Fanning, C.M., Luyendyk, B.P., 2004. Ross Sea mylonites and the timing of intracontinental extension within the West Antarctic rift system. Geology 32 (1), 57–60. https://doi.org/10.1130/G20005.1.
Smellie, J.L., Martin, A.P., 2021. Erebus Volcanic Province: Volcanology. In: Smellie, J.L., Panter, K.S., Geyer, A. (Eds.), Volcanism in Antarctica: 200 Million Years of Subduction, Rifting and Continental Break-Up. Geol. Soc. Lond. Memoirs. https://doi.org/10.1144/M55-2018-62.
Smellie, J.L., Rocchi, S., 2021. Northern Victoria LandVL: Volcanology. In: Smellie, J.L., Panter, K.S., Geyer, A. (Eds.), Volcanism in Antarctica: 200 Million Years of Subduction, Rifting and Continental Break-Up. Geol. Soc. Lond. Memoirs. https://doi.org/10.1144/M55-2018-60.
Spector, P., Balco, G., 2021. Exposure-age data from across Antarctica reveal mid-Miocene establishment of polar desert climate. Geology 49, 91–95. https://doi.org/10.1130/G47783.1.
Stephenson, R.A., Nakiboglu, S.M., Kelly, M.A., 1989. Effects of asthenosphere melting, regional thermoisostasy, and sediment loading on the thermomechanical subsidence of extensional sedimentary basins. Geophys. Monogr. 48, 17–27.
Sternai, P., 2020. Surface processes forcing on extensional rock melting. Sci. Rep. 10 https://doi.org/10.1038/s41598-020-63920-w.
Sternai, P., 2023. Feedbacks between internal and external dynamics. In: Duarte, J. (Ed.), Dynamics of Plate Tectonics and Mantle Convection. Elsevier. https://doi.org/10.1016/B978-0-323-85733-8.00019-6.
Sternai, P., Caricchi, L., Castelltort, S., Champagnac, J.D., 2016. Deglaciation and Glacial erosion: A Joint Control on Magma Productivity by Continental Unloading. Geophys. Res. Let. https://doi.org/10.1002/2015GL067285.
Sternai, P., Caricchi, L., Pasquero, C., Garzanti, E., van Hinsbergen, D.J.J., Castelltort, S., 2020. Magmatic Forcing of Cenozoic climate? J. Geophys. Res. Solid Earth 125. https://doi.org/10.1029/2018JB016460.
Sternai, P., Muller, V.A.P., Jolivet, L., Garzanti, E., Corti, G., Pasquero, C., Sembroni, A., Faccenna, C., 2021. Effects of asthenospheric flow and orographic precipitation on continental rifting. Tectonophysics 820. https://doi.org/10.1016/j.tecto.2021.229120.
Storey, B.C., Leat, P.T., Weaver, S.D., Pankhurst, R.J., Bradshaw, J.D., Kelley, S., 1999. Mantle plumes and Antarctica-New Zealand rifting: evidence from mid-cretaceous mafic dykes. J. Geol. Soc. London 156, 659–671. https://doi.org/10.1144/gsjgs.156.4.0659.
Stüwe, K., Robl, J., Turab, S.A., Sternai, P., Stuart, F.M., 2022. Feedbacks between sea-floor spreading, trade winds and precipitation in the Southern Red Sea. Nat. Commun. 13 https://doi.org/10.1038/s41467-022-32293-1.
Sugden, D., Denton, G., 2004. Cenozoic landscape evolution of the Convoy Range to Mackay Glacier area, Transantarctic Mountains: Onshore to offshore synthesis. GSA Bull. 116 (7–8), 840–857. https://doi.org/10.1130/B25356.1.
Tankersley, M.D., Horgan, H.J., Siddoway, C.S., Caratori Tontini, F., Tinto, K.J., 2022. Basement Topography and Sediment Thickness beneath Antarctica's Ross Ice Shelf. Geophys. Res. Letters 49, e2021GL097371. https://doi.org/10.1029/2021GL097371.
ten Brink, U.S., Hackney, R.I., Bannister, S., Stern, T.A., Makovsky, Y., 1997. Uplift of the Transantarctic Mountains and the bedrock beneath the East Antarctic ice sheet. J. Geophys. Res. Solid Earth 102, 27603–27621. https://doi.org/10.1029/97jb02483.
Tinto, K.J., Padman, L., Siddoway, C.S., et al., 2019. Ross Ice Shelf response to climate driven by the tectonic imprint on seafloor bathymetry. Nat. Geosci. 12, 441–449. https://doi.org/10.1038/s41561-019-0370-2.
Turcotte, D., Schubert, G., 2016. Geodynamics. Cambridge University Press. https://doi.org/10.1017/CBO9780511843877.
van der Beek, P., Andriessen, P., Cloetingh, S., 1995. Morphotectonic evolution of rifted continental margins: Interferences from a coupled tectonic-surface processes model and fission track thermochronology. Tectonics 14, 406–421. https://doi.org/10.1029/94TC02445.
van Wijk, J.W., Cloetingh, S.A.P.L., 2002. Basin migration caused by slow lithospheric extension. Earth Planet. Sci. Lett. 198, 275–288. https://doi.org/10.1016/S0012-821X(02)00560-5.
van Wijk, J.W., Huismans, R.S., ter Voorde, M., Cloetingh, S.A.P.L., 2001. Melt generation at volcanic continental margins: no need for a mantle plume? Geophys. Res. Lett. 28, 3995–3998. https://doi.org/10.1029/2000GL012848.
Verret, M., Trinh-Le, C., Dickinson, W., Norton, K., Lacelle, D., Christl, M., Levy, R., Naish, T., 2023. Late Miocene onset of hyper-aridity in East Antarctica indicated by meteoric beryllium-10 in permafrost. Nat. Geosci. https://doi.org/10.1038/s41561-023-01193-4.
Viereck, L.G., 1988. Origin of the Paleogene Vøring Plateau volcanic sequence. Geol. Soc. Spec. 39 (11), 69–83.
Vignaroli, G., Balsamo, F., Giordano, G., Rossetti, F., Storti, F., 2015. Miocene-to-Quaternary oblique rifting signature in theWestern Ross Sea from fault patterns in the McMurdo Volcanic Group, North Victoria Land, Antarctica. Tectonophysics 656, 74–90. https://doi.org/10.1016/j.tecto.2015.05.02.
Watts, A.B., 2001. Isostasy and Flexure of the Lithosphere. Cambridge University Press.
White, R., McKenzie, D., 1989. Magmatism at rift zones: the generation of volcanic continental margins and flood basalts. J. Geophys. Res. 94, 7685–7729. https://doi.org/10.1029/JB094iB06p07685.
Wilson, D.S., Luyendyk, B.P., 2009. West antarctic paleotopography estimated at the eocene-oligocene climate transition. Geophys. Res. Lett. 36 https://doi.org/10.1029/2009GL039297.
Ziegler, P.A., Cloetingh, S., 2004. Dynamic processes controlling evolution of rifted basins. Earth Sci. Rev. 64, 1–50. https://doi.org/10.1016/S0012-8252(03)00041-2.